

Article

Wood- and Cable-Based Variable Tilt Stilt-Mounted Solar Photovoltaic Racking System

Uzair Jamil ¹, Nicholas Vandewetering ², Seyyed Ali Sadat ³ and Joshua M. Pearce ^{3,4,*}

¹ Department of Mechanical and Materials Engineering, Western University, London, ON N6A 3K7, Canada; ujamil@uwo.ca

² Department of Civil and Environmental Engineering, Western University, London, ON N6A 3K7, Canada; nvandew@uwo.ca

³ Department of Electrical and Computer Engineering, Western University, London, ON N6A 3K7, Canada; ssadat6@uwo.ca

⁴ Ivey School of Business, Western University, London, ON N6A 3K7, Canada

* Correspondence: joshua.pearce@uwo.ca

Abstract: The prohibitive costs of small-scale solar photovoltaic (PV) racks decrease PV adoption velocity. To overcome these costs challenges, an open hardware design method is used to develop two novel variable tilt racking designs. These are the first stilt-mounted racking designs that allow for the manual change of the tilt angle from zero to 90 degrees by varying the length of cables. The racks are designed using the calculated dead, wind, and snow loads for Canada as a conservative design for most of the rest of the world. Structural capacities of the wooden members are then ascertained and the resisting bending moment, shear force, tensile force, and compressive force is calculated for them. A structural and truss analysis is performed to ensure that the racking design withstands the applicable forces. Moreover, the implications of changing the tilt angle on the wooden members/cables used to build the system are also determined. The systems offer significant economic savings ranging from one third to two thirds of the capital expenses of the commercially available alternatives. In addition, the racking designs are easy-to-build and require minimal manufacturing operations, which increases their accessibility. The stilt-mounted designs can be employed for agrivoltaic settings while allowing farm workers shaded, ergonomic access to perform planting, weeding, and harvesting.

Keywords: open source; photovoltaic; racking; solar energy; biomaterials; wood; photovoltaic; mechanical design; balance of systems; renewable energy



Citation: Jamil, U.; Vandewetering, N.; Sadat, S.A.; Pearce, J.M. Wood- and Cable-Based Variable Tilt Stilt-Mounted Solar Photovoltaic Racking System. *Designs* **2024**, *8*, 6. <https://doi.org/10.3390/designs8010006>

Academic Editor: Julian D. Booker

Received: 1 December 2023

Revised: 18 December 2023

Accepted: 5 January 2024

Published: 9 January 2024



Copyright: © 2024 by the authors. Licensee MDPI, Basel, Switzerland. This article is an open access article distributed under the terms and conditions of the Creative Commons Attribution (CC BY) license (<https://creativecommons.org/licenses/by/4.0/>).

1. Introduction

Solar photovoltaic (PV) technology has been established as a means to maintain our energy-intensive standard of living, while shifting society to a sustainable state [1]. The primary impediment to this transition has been economic, but PV technology has consistently dropped in price for decades [2,3] to the point that the solar levelized cost of electricity (LCOE) [4] is the lowest-cost option at both small and large scales [5,6]. Low-cost carbon-free solar electricity has made PV the most rapidly expanding source of electricity [6,7] and the true dominant new source of power [8]. Although PV at the large-scale is often the core focus of energy policy [9], to achieve the UN's 'Sustainable Energy for All' goals, small-scale single-family-home PV systems can play a major role [10] as they save consumers money [11]. The economics advantage of solar power is even more robust when the entire value of solar (VOS) is determined [12,13]. Despite the fact that PV generally provides economic benefit, the initial capital expenditures (CAPEX) of PV systems present a barrier to consumers in both developing [14,15] and developed economies [16,17].

Although large-scale industrial-based PV costs have been the lowest and dominate the market [9], small-scale, open-source, do-it-yourself (DIY) or even 'plug-and-play' solar [18]

can have costs that are lower than large scale systems. In general, the larger a system, the lower the cost per unit power [19]. This is because a substantial fraction of a PV system's cost is still soft costs (e.g., regulatory costs) that are the same or similar regardless of scale. Thus, there is a need to change the regulation in order to enable small-scale PV systems to meet their full potential [20–22] as, in aggregate, such systems could have a massive environmental and economic benefit [23].

Most of the de lines in PV system costs have come from the PV modules, while there has been very little progression in the balance of systems (BOS), which includes the racking, electronics, and wiring [3,24,25]. Simple mechanical racking dominates the costs of small PV systems, and proprietary and costly aluminum extrusion profiles have barely reduced costs [26]. To put this into perspective, PV module spot prices are currently USD 0.125/W [27], so an approximately 1 kW system would cost USD 125 while a three-module rack costs USD 459 [28], which is triple the PV cost, and a three-module pole mount racking systems costs USD 1312 [29], which is nine times the cost of the PV modules.

These prohibitive costs of small-scale racks make it very challenging for small system potential owners to participate in some of the most interesting and fastest growing areas of PV like agrivoltaics [30,31]. Agrivoltaics is the dual use of land for the purpose of agriculture and solar PV electricity generation [32–37]. The racking structures used for agrivoltaics, such as the stilt-mounted configurations, increase the cost of racking structure [36,38], which increases the differential cost per unit power between small and large system owners even further. These racks require more material due to increased height, thus there is a critical need to reduce the capital costs.

An effective means to reduce PV racking costs is to use open source hardware for the distributed production of racking including: (i) low-tilt angle racks for mobile PV arrays [39], (ii) cable-based X-wire PV racking systems for both flat commercial rooftops [40], as well as (iii) ground-mounted PV systems near the equator [41], (iv) tensegrity-based PV racking [42], (v) after-market building integrated PV (BIPV) [43], (vi) fixed-tilt ground-mounted wood racking [44], (vii) variable-tilt wood racking [45], (viii) vertically mounted wood racking PV systems [46], (ix) fence-based PV systems [47], (x) aftermarket floatovoltaics [48], (xi) trellis-based agrivoltaics racking [49], and a (xii) cable- and pipe-based mobile photovoltaic racking [50]. No racking design, however, has focused on agrivoltaics as well as normal PV along with the flexibility of changing tilt angle manually with stilt-mounted systems in the literature.

To fill this knowledge gap, this study proposes two novel low-cost, sustainable, easy-to-build, variable tilt racking designs. These are the first stilt-mounted racking designs that allow the manual change of tilt angle by varying the length of cables. The racks are designed using the calculated dead, wind, and snow loads for Canada as a conservative design for most of the rest of the world. Structural capacities of the wooden members are then ascertained and the resisting bending moment, shear force, tensile force, and compressive force for them are calculated. A structural and truss analysis is performed to ensure that the racking design withstands the applicable forces. Moreover, implications of changing the tilt angle on the wooden members/cables used to build the system is also determined. The results are reviewed and discussed for the novel racking systems applications in agrivoltaics, fencing, and parking lots/street parking as they can provide shade to automobiles.

2. Materials and Methods

2.1. Selection of Wood and Wire Rope

The primary construction materials for the racking design is wood due to its widespread availability and sustainability [51]. While growing wood absorbs carbon dioxide, it can be repurposed/recycled after its primary uses or can be utilized as biofuel [52]. In comparison with other racking materials, wood has lower energy requirements for processing which translates into a negative embodied energy and carbon footprint [53]. When compared to a ton of steel, softwood required 24 times less energy for the same mass [53]. Aluminum, a commonly used material for PV racks, has over five times the embodied CO₂e/kg of

wood [54]. Moreover, using wood as a construction material for PV module mounting structure also has distinct economic benefits, especially in North America [55]. In addition, to hold as well as to provide the option of changing the tilt angle of PV modules, wire rope is being used. Wire has been used before in x-wire-based low-tilt angle racking systems [40] and tensegrity racking [42]. Here, its primary function will be to vary the tilt angle of the array while enabling flexibility to ensure smaller members are able to be used for a given wind load.

2.2. Dimensional and Mechanical Characteristics of Wooden Members and Cables

Table 1 provides a summary of the dimensional and mechanical properties of the wooden members. It is of the utmost importance that, during construction, the base of any member should be smaller than its height. This ensures that the lumber is loaded along its strong axis, leading to an optimal moment of inertia and the first moment of area.

Table 1. Dimensional characteristics of wood used for the racking.

| Lumber | Lumber Breadth 'b' (m) | Lumber Height 'h' (m) | Area 'A' (m ²) A = bh | Moment of Inertia 'I' (m ⁴) I = bh ³ /12 | First Moment of Area 'Q' (m ³) Q = hA/8 |
|--------|------------------------|-----------------------|--------------------------------------|--|--|
| 2 × 12 | 0.038 | 0.286 | 0.010868 | 7.4079 × 10 ⁻⁵ | 3.8853 × 10 ⁻⁴ |
| 2 × 4 | 0.038 | 0.089 | 0.003382 | 2.2324 × 10 ⁻⁶ | 3.7624 × 10 ⁻⁵ |
| 2 × 6 | 0.038 | 0.140 | 0.005320 | 8.6893 × 10 ⁻⁶ | 9.3100 × 10 ⁻⁵ |
| 2 × 8 | 0.038 | 0.184 | 0.006992 | 1.9726 × 10 ⁻⁵ | 1.6081 × 10 ⁻⁴ |
| 2 × 10 | 0.038 | 0.235 | 0.008930 | 4.1096 × 10 ⁻⁵ | 2.6232 × 10 ⁻⁴ |
| 6 × 6 | 0.140 | 0.140 | 0.019600 | 3.2013 × 10 ⁻⁵ | 3.4300 × 10 ⁻⁴ |

Table 2 provides the breaking strength and work load for galvanized aircraft cable [56] used as a construction material. Other cables with similar strength can also be used.

Table 2. Breaking strength and workload for galvanized aircraft cable in lbs and N in parentheses.

| Diameter—Inches (m) | Breaking Strength—lbs. (N) | Approx. Wt./1000 ft | Workload Limit—lbs. (N) |
|---------------------|----------------------------|---------------------|-------------------------|
| 1/16 (0.0016) | 480 (2135) | 0.75 | 96 (427) |
| 3/32 (0.0024) | 1000 (4448) | 16.5 | 200 (890) |
| 1/8 (0.0032) | 2000 (8896) | 29 | 400 (1779) |
| 5/32 (0.0040) | 2800 (12,455) | 45 | 560 (2491) |
| 3/16 (0.0048) | 4200 (18,682) | 65 | 840 (3736) |
| 7/32 (0.0056) | 5600 (24,910) | 86 | 1120 (4982) |
| 1/4 (0.0064) | 7000 (31,138) | 110 | 1400 (6228) |
| 5/16 (0.0079) | 9800 (43,592) | 173 | 1960 (8718) |
| 3/8 (0.0095) | 14,400 (64,054) | 243 | 2880 (1281) |

2.3. PV Racking Design Parameters

For designing the PV rack, 460 W rated 144 HC M6 Bifacial Module [57] is selected. Using a bifacial PV module increases the electrical output [58,59], as well as assists clearing snow on the front side of the PV module [60,61]. The modules have dimensions of 2108 mm × 1048 mm. If modules with different measurements are used, the design can be adjusted to meet specific module requirements. The proposed racking design has a height of approximately 1.8 m above the ground, ensuring a 500 mm ground clearance—sufficient for snow sliding, even in the most extreme northern atmospheres [62]. A case study is presented where the racking structure is specifically designed for London, Ontario, with a latitude and longitude of 42.9849° N and 81.2453° W.

2.4. Main Design

2.4.1. T-Shaped Wood and Cable Design

The racking design consists of two posts, 140 mm × 140 mm in cross section. The height of the posts is 1848 mm above the ground with approximately 1200 mm under the

ground forming the foundation of the rack. One beam, 38 mm × 286 mm in cross section, is attached to the posts to hold one end of the PV module. The other end of the module is held via 3/8" galvanized aircraft cable from the two sides [63]. Changing the length of the wire enables the change in the tilt angle of the modules. The analysis is performed with cables that are assumed to be making a 15° angle with the horizontal. Two modules are held between the two posts. Figure 1 shows the assembly of the structure with labelling.

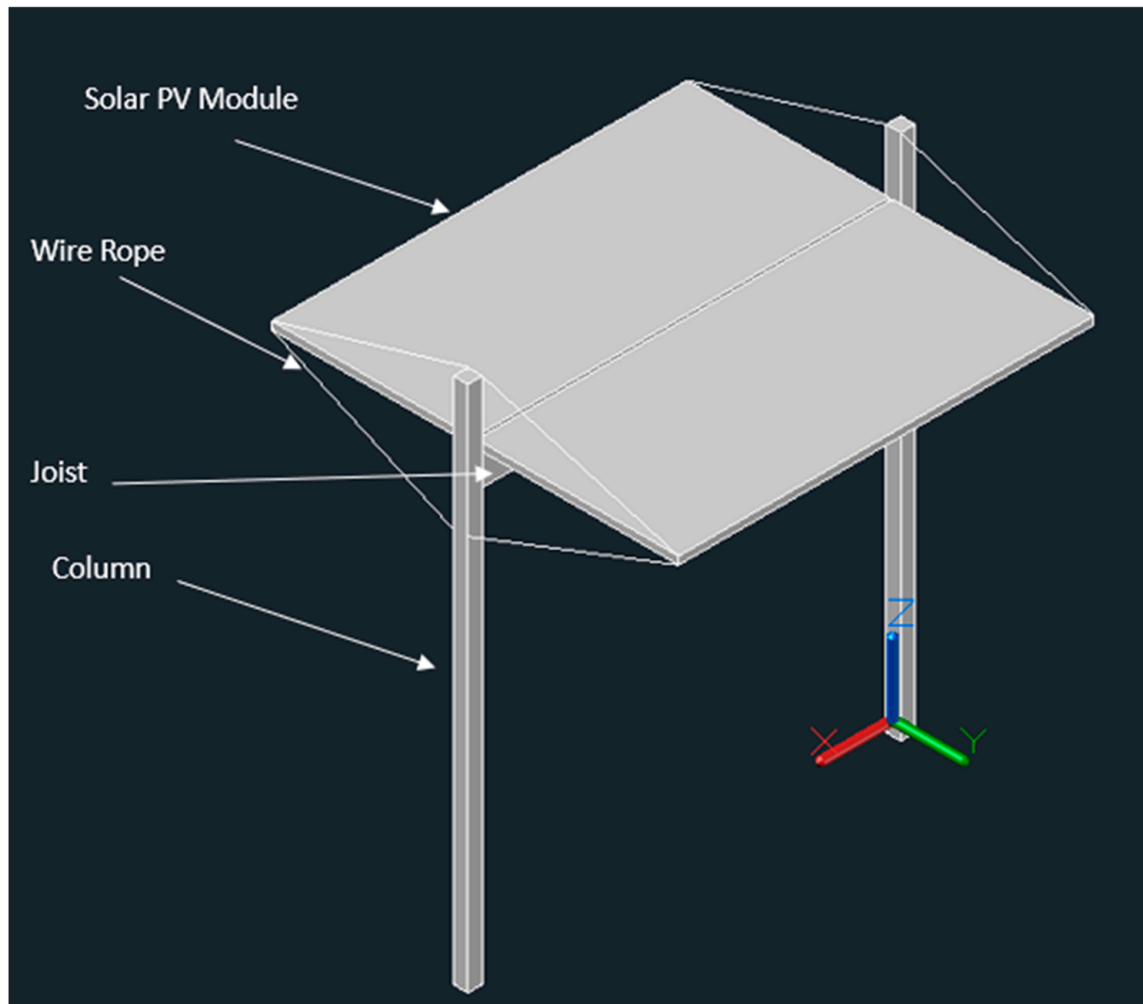


Figure 1. Wood- and cable-based variable tilt solar photovoltaic racking system.

2.4.2. Cantilevered Carport Wood and Cable Design

The structure consists of two posts, 184 mm × 184 mm in cross section. As for the T-shaped design, the height of the posts is 1848 mm above the ground wit. One beam, 38 mm × 140 mm in cross section, is attached to the posts to hold one end of the PV module. The other end of the module is held via 3/8" galvanized aircraft cable from the two sides [63]. Changing the length of the wire enables the change in the tilt angle of the modules. The analysis is performed with cables assumed to be making a 15° angle with the horizontal. A single module is cantilevered between two posts. Figure 2 shows the assembly of the structure with labelling.

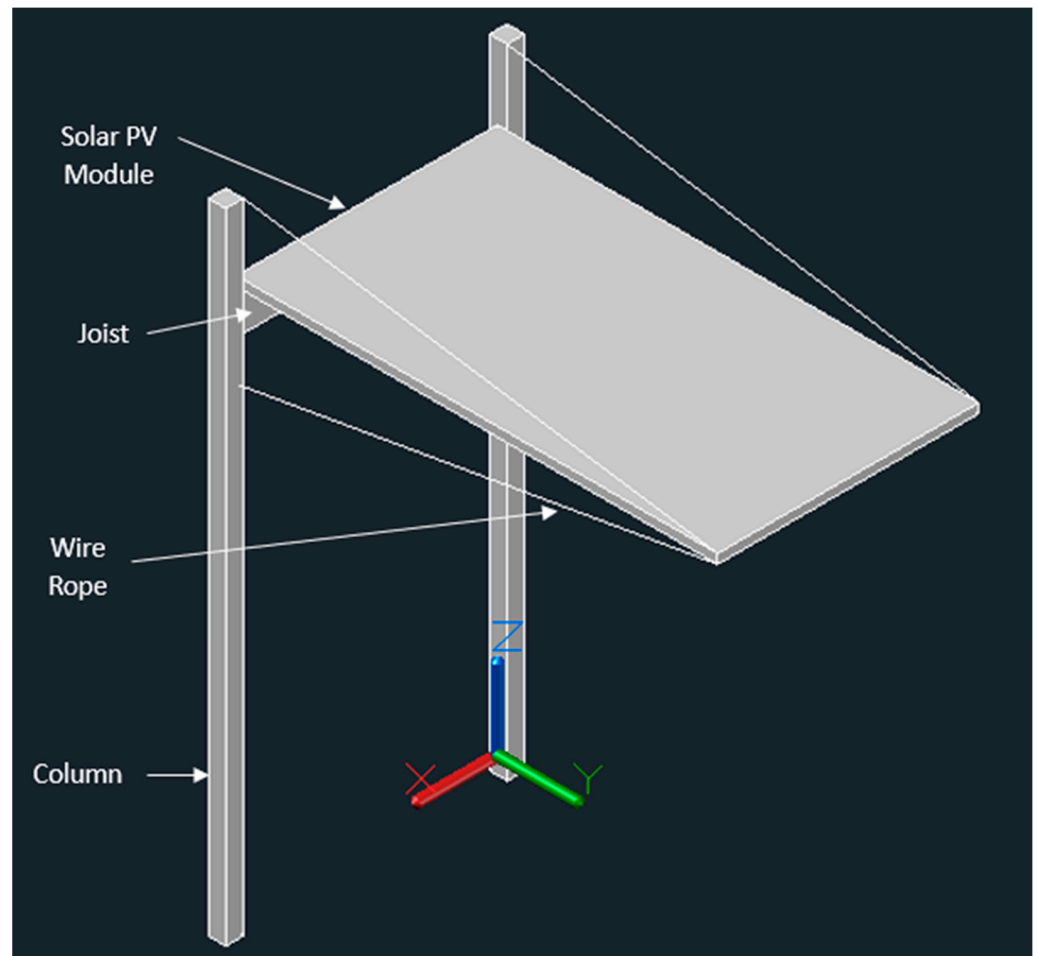


Figure 2. Cantilevered system with single module.

A variation of this configuration is the two-module cantilevered design where the modules are cantilevered on each side of the center joist. The same 184 mm × 184 mm posts are used in this design as well; however, the center joist requires more strength. The structural and truss analysis for this design becomes identical to the two module T-shaped design where a 38 mm × 284 mm wooden member is used to hold the load acting on both the modules. Refer to Figure 3 for the assembly of the racking structure.

For both the designs, changing the angle of wire rope influences the tension it experiences. The cables are attached to the wooden members through sheep eye hook screws while cable clamps are also used to close out the ends of the cables. Different lengths of cables can be used to change the tilt angle of the solar modules, or a turnbuckle can also be used for the same reason. The force experienced by the cable when tied at different angles is ascertained for every 5° angle increment. Moreover, changing the tilt angle of modules changes the loading on the structure, and its subsequent impact on wooden member(s) used in each design is also determined.

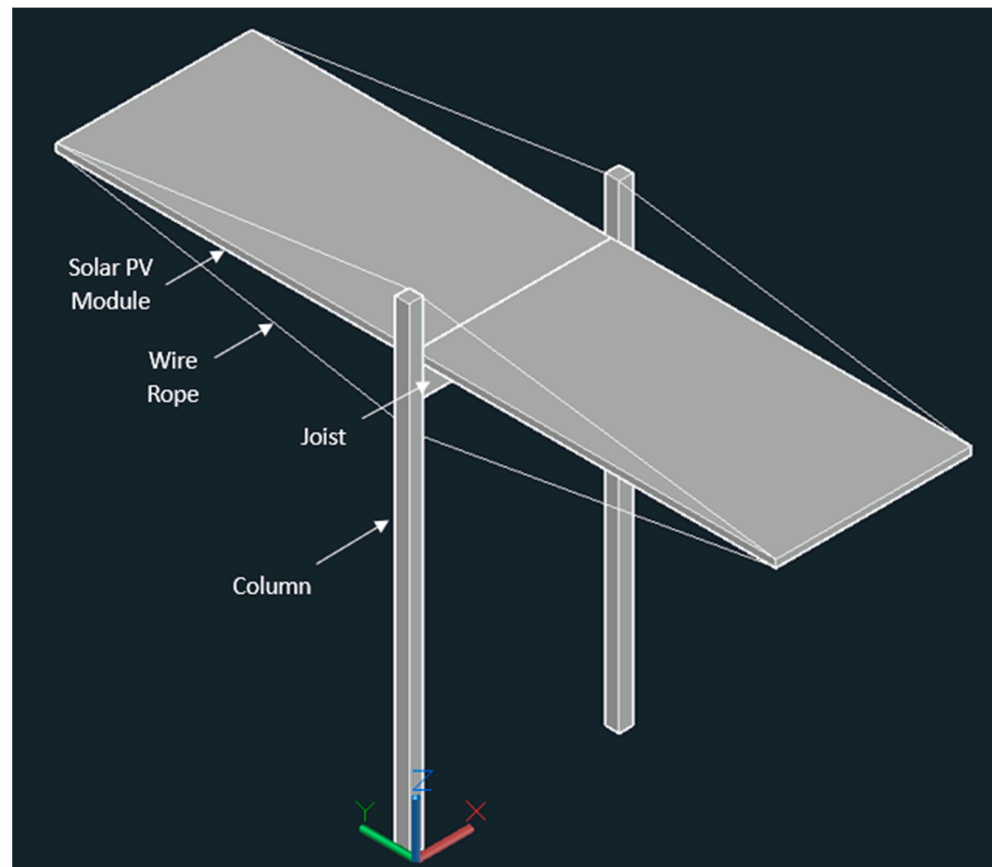


Figure 3. Cantilevered system with two modules.

2.5. Bill of Materials (BOM)

The bill of materials (BOM) of the T-shaped design is shown in Table 3.

Table 3. Bill of materials (BOM) for wood and cable-based T-shaped variable tilt solar photovoltaic racking system (horizontal modules with cable making 19° angle).

| Member Name | Piece ¹ | Cost per Piece (CAD) ² | Quantity | Cost (CAD) |
|---|----------------------------------|-----------------------------------|----------|------------|
| Joists | 2 × 12 × 8 | 35.00 | 1 | 35.00 |
| Posts | 6 × 6 × 10 | 52 | 2 | 104.00 |
| Joist to Post Connection | 2 × 4 Fence Bracket | 0.43 | 2 | 0.86 |
| 7 × 19 PVC Coated and Galvanized Aircraft Cable | 3/8" | 55.44 | 1 | 55.44 |
| Connections | 2-1/2" Brown Deck Screws | 2.61 | 1 | 2.61 |
| Cable Clamp | 5/16" Wire Rope Clip—Zinc Plated | 1.99 | 16 | 31.84 |
| Turnbuckle | 9-3/8 Turnbuckle | 6.94 | 4 | 27.76 |
| Hooks | 4-3/8 Hooks | 5.22 | 8 | 41.76 |
| Washers | 1/4 Washers | 1.90 | 1 | 1.90 |
| Eye Bolts | 1/4 × 2 Eye Bolts | 1.72 | 8 | 13.76 |
| Hinges | Light duty (2") | 2.69 | 4 | 10.76 |
| Nut and Bolt | 1/4 inch | 2.78 | 1 | 2.78 |
| Metal fixture | 2" | 8.49 | 1 | 8.49 |
| Total Cost with No Concrete | | | | 336.95 |
| Concrete for Posts | 30 MPa Quikrete concrete | 6.38 | 10 bags | 63.80 |
| Total Cost: | | | | 400.75 |

¹ All lumber is to be pressure treated, and all hardware is to be hot-dipped galvanized. ² All costs are in Canadian Dollars as of 15 October 2023, before tax.

The bill of materials (BOM) of the carport design is given in Tables 4 and 5.

Table 4. Bill of materials (BOM) for wood and cable-based variable tilt carport design with one module (horizontal modules with cable making 19° angle).

| Member Name | Piece ¹ | Cost per Piece (CAD) ² | Quantity | Cost (CAD) |
|---|----------------------------------|-----------------------------------|----------|------------|
| Joists | 2 × 6 × 8 | 12.78 | 1 | 12.78 |
| Posts | 8 × 8 × 10 | 125.33 | 2 | 250.66 |
| Joist to Post Connection | 2 × 4 Fence Bracket | 0.43 | 2 | 0.86 |
| 7 × 19 PVC Coated and Galvanized Aircraft Cable | 3/8" | 55.44 | 1 | 55.44 |
| Connections | 2-1/2" Brown Deck Screws | 2.61 | 1 | 2.61 |
| Cable Clamp | 5/16" Wire Rope Clip—Zinc Plated | 1.99 | 8 | 15.92 |
| Turnbuckle | 9-3/8 Turnbuckle | 6.94 | 2 | 13.88 |
| Hooks | 4-3/8 Hooks | 5.22 | 4 | 20.88 |
| Washers | 1/4 Washers | 1.90 | 1 | 1.90 |
| Eye Bolts | 1/4 × 2 Eye Bolts | 1.72 | 4 | 6.88 |
| Hinges | Light duty (2") | 2.69 | 2 | 5.38 |
| Nut and Bolt | 1/4 inch | 2.78 | 1 | 2.78 |
| Metal Fixture | 2" | 8.49 | 1 | 8.49 |
| Total Cost with No Concrete | | | | 398.45 |
| Concrete for Posts | 30 MPa Quikrete concrete | 6.38 | 10 bags | 63.80 |
| Total Cost: | | | | 462.25 |

¹ All lumber is to be pressure treated, and all hardware is to be hot-dipped galvanized. ² All costs are in Canadian Dollars as of 15 October 2023, before tax.

Table 5. Bill of materials (BOM) for wood and cable-based variable tilt carport design with two modules (horizontal modules with cable making 15° angle).

| Member Name | Piece ¹ | Cost per Piece (CAD) ² | Quantity | Cost (CAD) |
|---|----------------------------------|-----------------------------------|----------|------------|
| Joists | 2 × 12 × 8 | 35.00 | 1 | 35.00 |
| Posts | 8 × 8 × 10 | 125.33 | 2 | 250.66 |
| Joist to Post Connection | 2 × 4 Fence Bracket | 0.43 | 2 | 0.86 |
| 7 × 19 PVC Coated and Galvanized Aircraft Cable | 3/8" | 110.88 | 1 | 110.88 |
| Connections | 2-1/2" Brown Deck Screws | 2.61 | 1 | 2.61 |
| Cable Clamp | 5/16" Wire Rope Clip—Zinc Plated | 1.99 | 16 | 31.84 |
| Turnbuckle | 9-3/8 Turnbuckle | 6.94 | 4 | 27.76 |
| Hooks | 4-3/8 Hooks | 5.22 | 8 | 41.76 |
| Washers | 1/4 Washers | 1.90 | 1 | 1.90 |
| Eye Bolts | 1/4 × 2 Eye Bolts | 1.72 | 8 | 13.76 |
| Metal Fixture | 2" | 8.49 | 1 | 8.49 |
| Nut and Bolt | 1/4 inch | 2.78 | 1 | 2.78 |
| Hinges | Light duty (2") | 2.69 | 4 | 10.76 |
| Total Cost with No Concrete | | | | 539.05 |
| Concrete for Posts | 30 MPa Quikrete concrete | 6.38 | 10 bags | 63.80 |
| Total Cost: | | | | 602.85 |

¹ All lumber is to be pressure treated, and all hardware is to be hot-dipped galvanized. ² All costs are in Canadian Dollars as of 15 October 2023, before tax.

Hardware components used to build the cable attachments are shown in Figure 4.

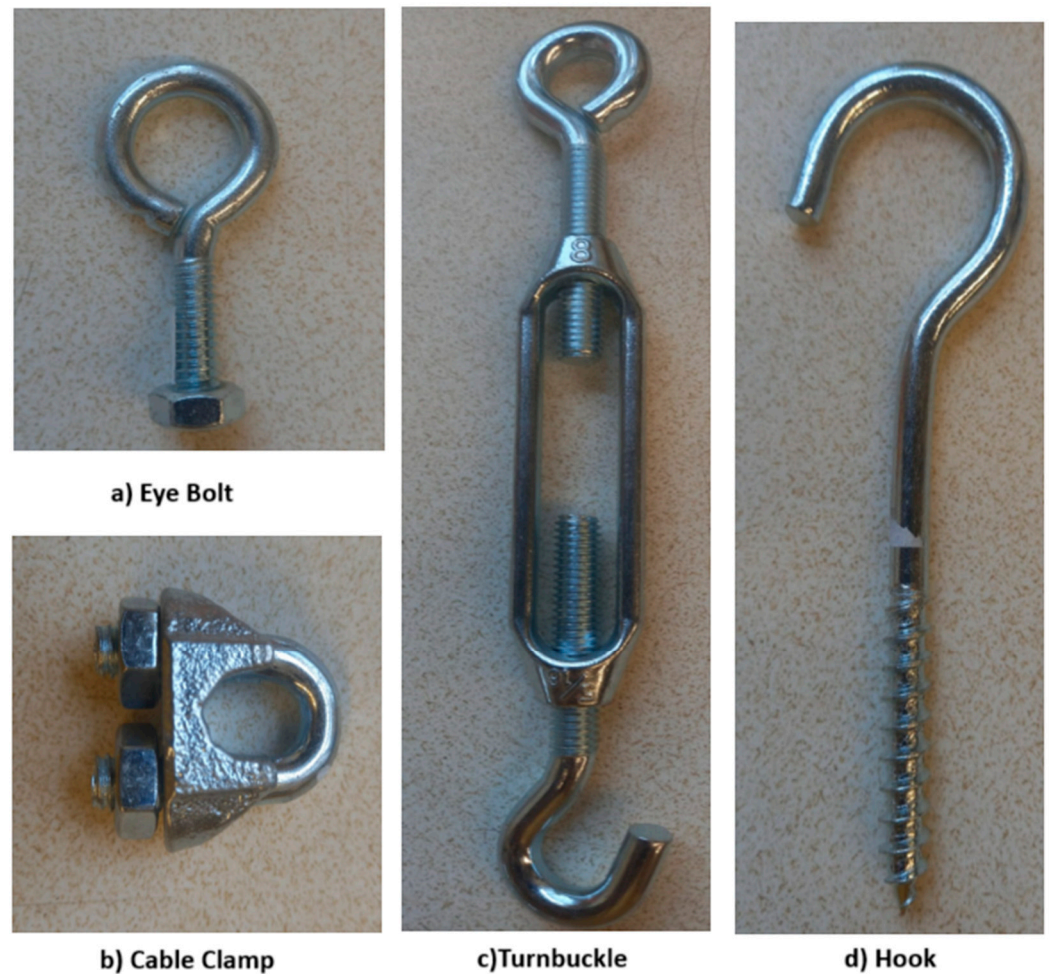


Figure 4. Attachments for cables.

2.6. Load Calculations

The load calculations including snow loads, wind loads, dead loads, and their combination are detailed in Appendix B. In addition, Appendix B provides the wooden members structural capacity and the structural analysis for the T-shaped racking design.

2.7. PV System Simulations

PV system simulations for the advantage of different fixed tilt angle adjustments throughout the year have been summarized previously [45].

2.8. Variables

All variables in this article are adopted from the Jamil et al. [49] trellis-based agri-voltaics racking design.

2.9. Finite Element Analysis (FEA)

FEA is performed to ascertain if the racking design will result in stress that exceeds the yield/design stress of the aluminum frame used to hold the PV modules on the mounting structure. FEA was performed utilizing Abaqus/CAE 2022 on a computer equipped with an eighth generation Core i7 CPU and 16 GB of RAM. The PV module FEA model similar to [64] is considered, as it simulates a standard configuration, and encompasses a PV aluminum frame, PV laminate (consisting of glass, solar cells, ethylene-vinyl acetate (EVA), and back sheet), and rubber components. The simulation conducted in Abaqus resembles the boundary conditions of three designs discussed in Section 2.4. The FEA analysis took into account the behavior of the rubber within the PV module, incorporating material

behaviors consistent with established research [65,66]. In the simulation, it was assumed that the rubber was bonded to the aluminum frame through tie constraints in Abaqus and, similarly, the laminate was attached to the rubber using tie constraints. Addressing the fasteners, one side of the PV module's length had the frame's bottom constrained in the Z direction to represent placement on a wooden rack, while a portion of the frame's bottom on the other side was fixed in the Z direction to simulate the fixture used for the PV module as demonstrated in Figure 5. In another model, the boundary conditions for fixtures on the PV module are removed to see how this affects the final results. In the main FEA model, the bolts under the bottom of PV aluminum frame were simulated following a methodology presented by [64] to model their boundary conditions. Also, in another simulation, in order to analyze an alternative configuration for mounting PV modules with no fixtures, the bolts were drilled from the sides of the PV frame as shown in Figure 6. The material properties for all components used in the FEA are outlined in Table 6. The simulations considered the weight of all components, acknowledging its significance in real-world applications.

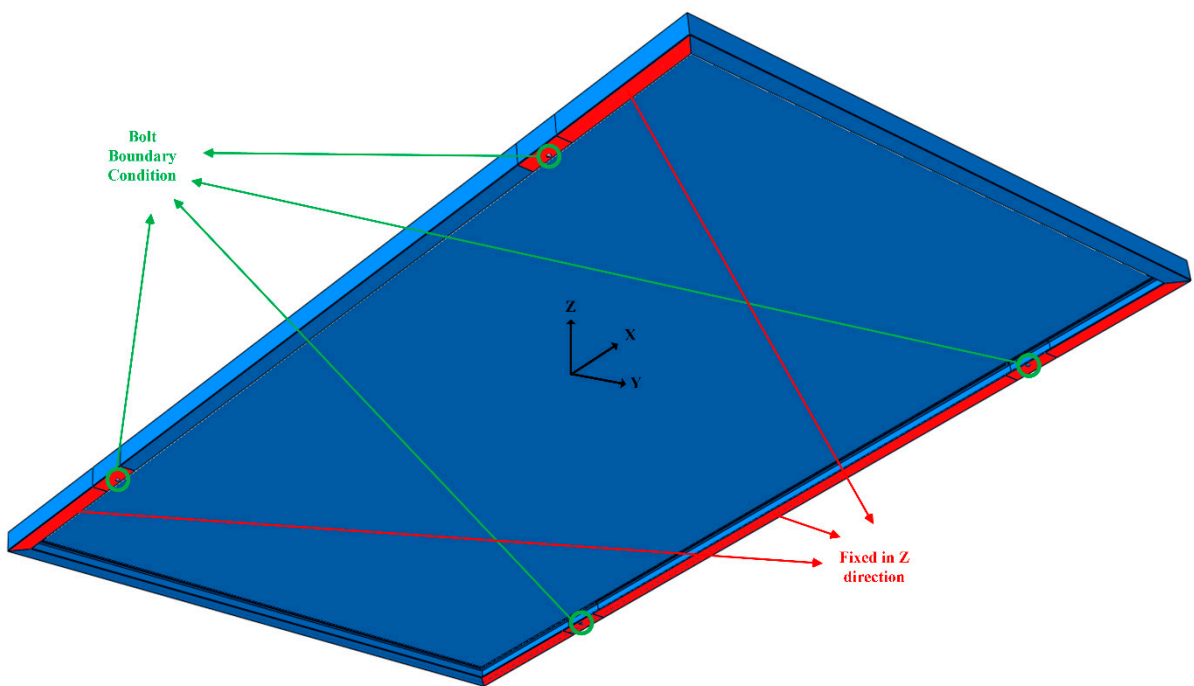


Figure 5. Boundary conditions for the main FEA model.

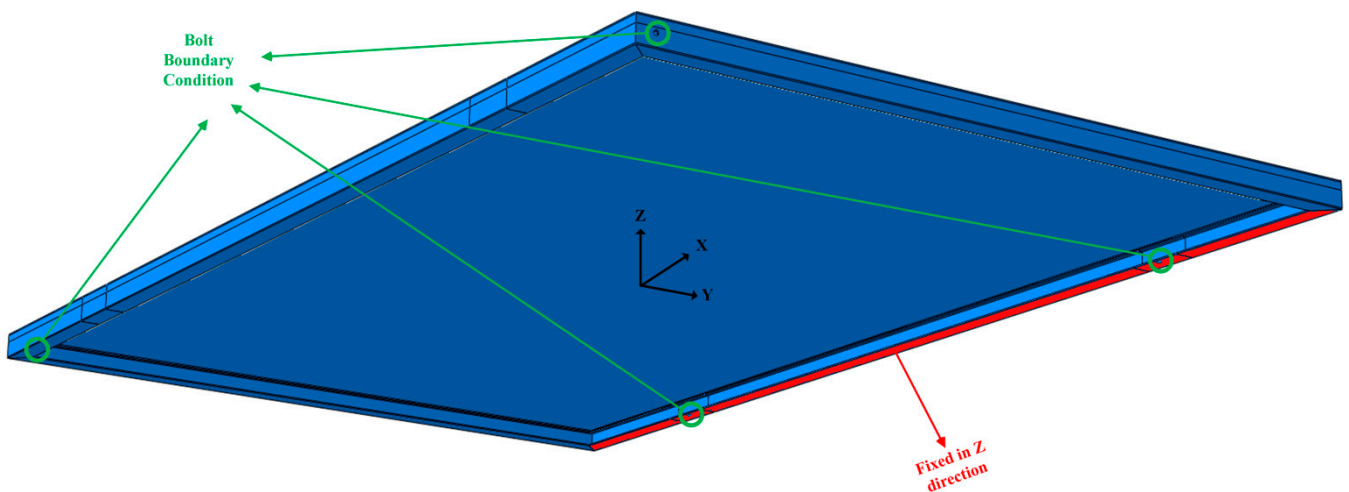


Figure 6. Boundary conditions for the side bolts FEA model.

For meshing, linear hexahedral mesh elements were employed, aligning with prior studies [64,66]. In all simulations, seed and element sizes were reduced as much as possible to constrain computational time based on available computational resources. To enhance the precision of the FEA results, various partitioning methods in Abaqus were utilized, facilitating the application of sweep and structured techniques for meshing all parts more efficiently. These methods were thoughtfully selected to eliminate any flawed or error-associated elements from the simulations, thereby bolstering the reliability of the findings. The collective considerations outlined above were implemented to ensure that the FEA results would closely align with real-world conditions and provide accurate insights.

Table 6. Materials and mechanical properties of parts used in FEA simulations.

| | Material | Thickness [mm] | Density [tonne/mm ³] | Young's Modulus [MPa] | Poisson's Ratio [64,66] | Strength [MPa] | Number of Elements |
|----------|---|----------------|----------------------------------|-----------------------|-------------------------|-------------------------------|--------------------|
| Frame | Aluminum (Alloy 6063 [64]) | 1.80 | 2.70×10^{-9} | 70,000 | 0.33 | 214 yield 241 tensile | 15,980 |
| Sealing | Rubber (Polyurethane elastomer [64]) | 2.00 | 6.70×10^{-11} | 7.40 | 0.30 | 0.0814–103 | 3654 |
| Laminate | Glass (soda-lime glass [64]) | 3.20 | 2.50×10^{-9} | 70,000 | 0.20 | Compressive Strength = 274 | 64,288 |
| | Solar cells (Czochralski silicon [64]) | 0.18 | 2.329×10^{-9} | 112,400 | 0.28 | Compressive Strength = 120 | |
| | Encapsulation (ethylene vinyl acetate [64]) | 0.45 | 9.6×10^{-10} | T-dep. | 0.40 | 3.4–10 | |
| | Back sheet (TPT [64]) | 0.22 | 2.52×10^{-9} | 3500 | 0.29 | Break stress = 132 | |

3. Results

3.1. Loads

3.1.1. Snow Loads

The snow load for London, ON, comes out to be 1.771 kPa following Equation (A1) up to a tilt of 15°. The snow load changes when the tilt of the module's changes. For a 30° tilt, it is 1.334 kPa, for 45°, it is 0.897 kPa and, for 60°, it is 0.460 kPa.

3.1.2. Wind Loads

Using Equations (A2)–(A4), the external pressure, the internal pressure, and the total wind load are found out to be −0.98 kPa, −0.68 kPa, and −1.66 kPa, respectively.

3.1.3. Dead Load

The CanmetENERGY research center at Natural Resources Canada [67] advises that the dead load of PV systems, commonly known as the superimposed dead load, should be accounted for as 0.24 kPa. For the weight of lumber, it is advisable to utilize the wooden member weight supplied by the supplier and transform it into a uniformly distributed load measured in kN/m.

3.1.4. Load Combination

The load combinations that yield the highest positive and negative values are given in Table 7.

Table 7. Wind, Snow, and Dead Load Combination.

| Load Combination | Load [kPa] (up to 15°) | Load [kPa] (30°) | Load [kPa] (up to 45°) | Load [kPa] (60°) |
|---------------------|------------------------|------------------|------------------------|------------------|
| 0.9D + 1.4W − 0.5S | −2.99 | −2.77 | −2.56 | −2.33 |
| 1.25D + 1.5S − 0.4W | 3.62 | 2.96 | 2.31 | 1.65 |

Given that all connections are capable of handling loads in both directions and all members exhibit similar material properties in both directions, the analysis for the negative case is essentially identical to the positive case. Consequently, there is no requirement to specifically evaluate both the cases, and the analysis will only be performed for the case which carries a higher load value.

3.2. Wooden Members Structural Capacity

In Canada, spruce pine fir grades 1 and 2 make up most of the pressure-treated wood used for construction and its mechanical properties [68] are given in Table 8.

Table 8. Structural properties for spruce pine fir wood.

| Factor | Value (MPa) |
|-----------|-------------|
| f_b | 6.03 |
| f_v | 0.93 |
| f_t | 3.10 |
| f_c | 7.93 |
| E | 9652.66 |
| E_{min} | 3516.33 |

Resistance factors are provided in Table 9.

Table 9. Resistance factors.

| Factor | Value |
|----------|---------------------|
| C_D | 1.15 |
| C_T | 1.00 |
| C_M | 1.00, 0.97 and 0.90 |
| C_L | 0.64, 0.76 |
| C_{fu} | 1.2 |
| C_i | 1, 0.8 and 0.95 |
| C_r | 1.00 |
| C_F | 1.10 |
| C_P | 0.29 |

Following Equations (A5)–(A10), the factored properties of pressure-treated spruce pine fir wood are given in Table 10. The table only shows the values for the most conservative case where the solar modules are placed horizontally.

Table 10. Factored structural properties for spruce pine fir wood.

| Factored Capacities | Value (MPa) |
|---------------------|-------------|
| f_b^* | 4.68 |
| f_v^* | 0.83 |
| f_t^* | 3.14 |
| f_c^* | 2.94 |
| E * | 8253.03 |
| E_{min}^* | 3006.46 |

* represents the factored structural properties.

The resistance values are next determined using the factored capacities calculated above as well as the dimensional properties of the lumber (Equations (A11)–(A14)). Table 11 summarizes the resisting values for differently sized wooden members when the solar modules are held horizontally on the structure.

Table 11. Resisting bending moment, shear force, tensile force, and compressive force for different members of spruce pine fir wood.

| Lumber | Resisting Bending Moment 'Mr' (kN-m) | Resisting Shear Force 'Vr' (kN) | Resisting Tensile Force 'Tr' (kN) | Resisting Compressive Force 'Cr' (kN) |
|--------|--------------------------------------|---------------------------------|-----------------------------------|---------------------------------------|
| 2 × 4 | 0.23 | 1.87 | 10.62 | 9.97 |
| 2 × 6 | 0.58 | 2.95 | 16.70 | 15.69 |
| 2 × 8 | 1.00 | 3.87 | 21.95 | 20.62 |
| 2 × 10 | 1.64 | 4.94 | 28.04 | 26.34 |
| 4 × 10 | 3.27 | 9.89 | 56.08 | 52.67 |
| 2 × 12 | 2.42 | 6.02 | 34.12 | 32.05 |
| 4 × 4 | 0.55 | 4.39 | 24.87 | 23.36 |
| 6 × 6 | 2.14 | 10.85 | 61.54 | 57.80 |

Subsequently, structural analysis is performed to ascertain optimal dimensions of wooden members required for the construction of a functional system.

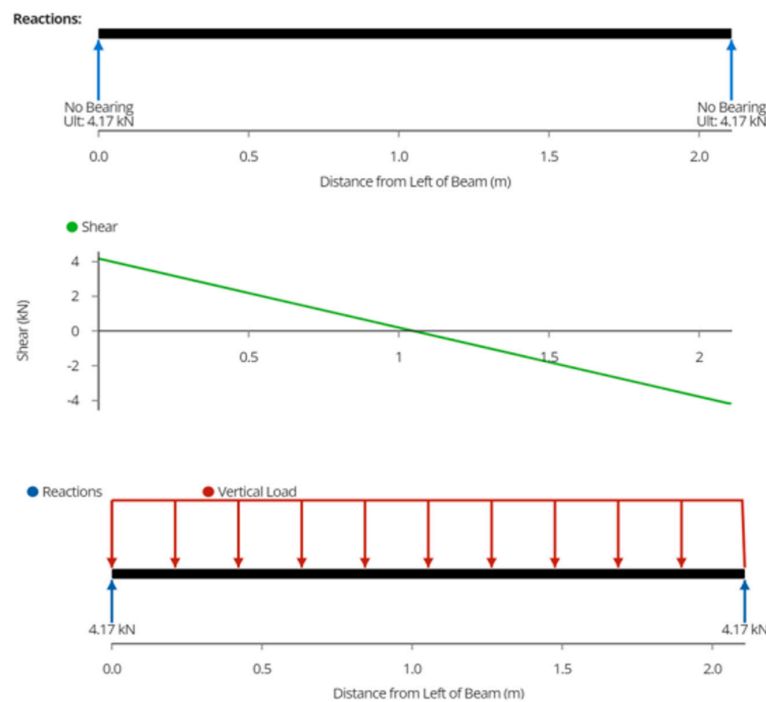
3.3. Structural Analysis

3.3.1. Joist

The joist connected with the two posts has a tributary width of 1.064 m for two module T-shaped designs and 1.054 m for cantilever design.

Total uniformly distributed for the joist comes out to be 3.96 kN/m and 3.93 kN/m for the two designs using Equation (A15).

Following Equation (A16), the maximum shear force or reaction is found out to be 4.18 kN for T-shaped variable tilt racking system and 2.05 kN for cantilever design (Figure 7).



(a)

Figure 7. Cont.

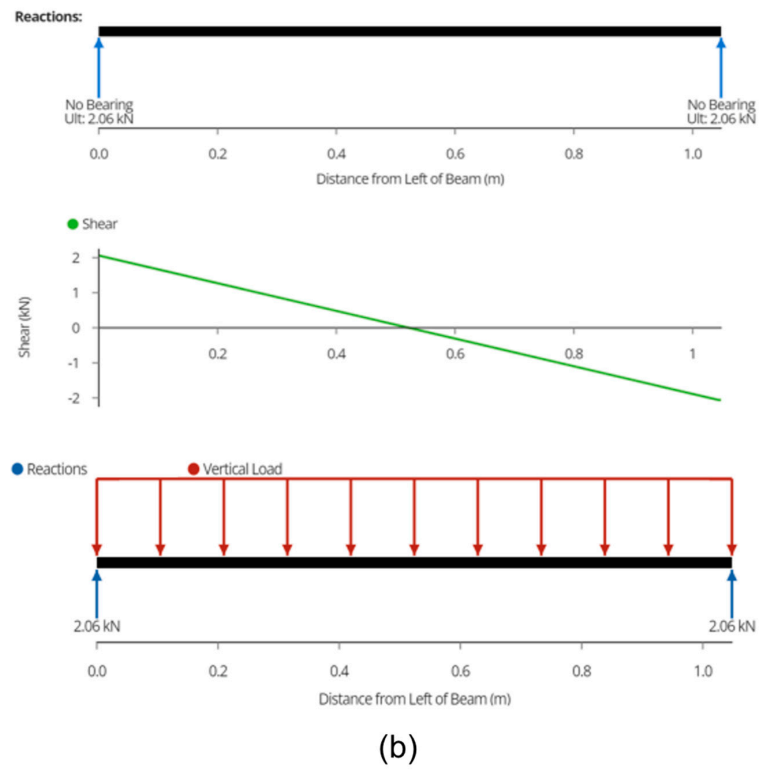


Figure 7. Reaction and Maximum Shear Forces (a) T-shaped and cantilever two module design, (b) Cantilever one module design.

Moreover, the bending moment is determined as 2.20 kN m and 0.54 kN m for the two structures from Equation (A17), as depicted in Figure 8.

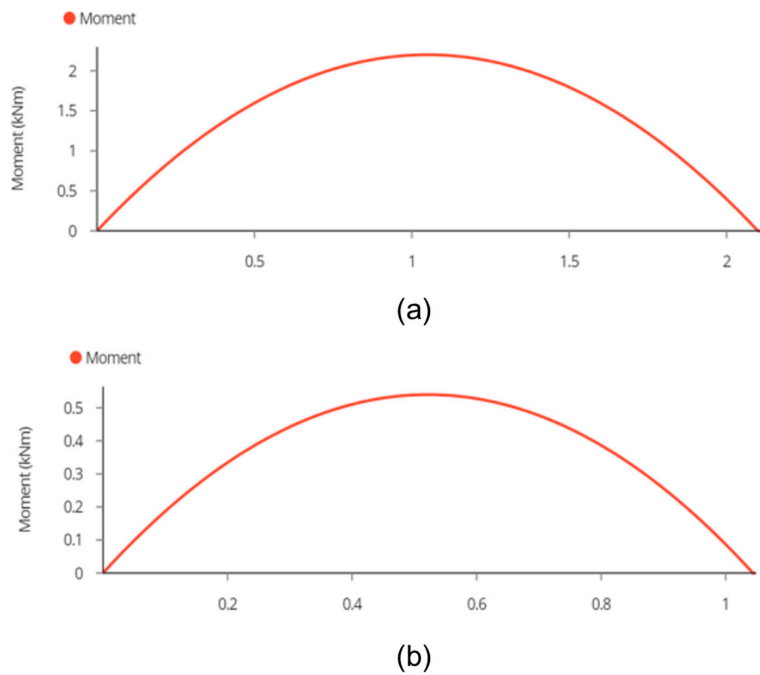


Figure 8. Bending Moment (a) T-shaped and cantilever two module design, (b) Cantilever one-module design.

Finally, the maximum deflection using Equation (A18) is ascertained as 1.42 mm and 0.086 mm for the two designs (Figure 9).

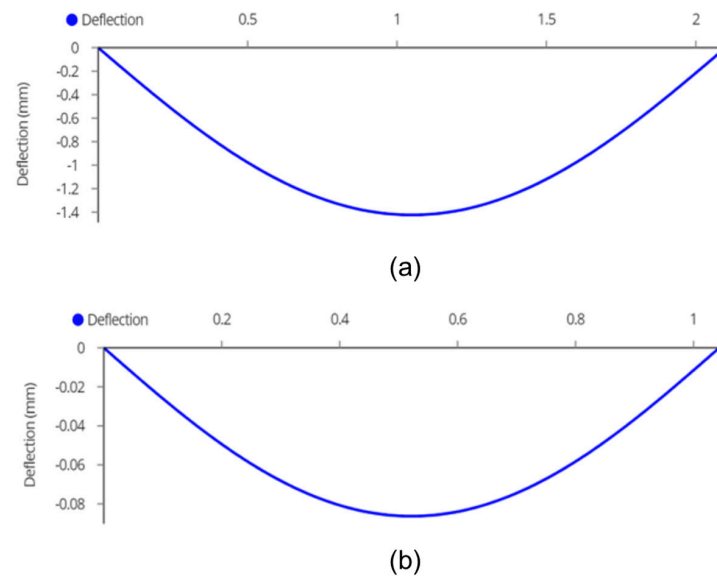


Figure 9. Maximum Deflection (a) T-shaped and cantilever two module design, (b) Cantilever one module design.

The structural analysis is performed for 30°, 45°, and 60° tilts of solar modules as well using the respective snow loads. For the two module T-shaped variable tilt racking design, the maximum shear or reaction is reduced to 3.44 kN, 2.96 kN, and 2.72 kN for the three angles on the center joist. The bending moment comes out to be 1.81 kN-m, 1.56 kN-m, and 1.43 kN-m, whereas the deflection is calculated as 1.17 mm, 1.01 mm, and 0.93 mm, respectively. This means that with 45° and 60° tilts, 2 × 10 pressure-treated wood can be used.

For the cantilever variable tilt racking configuration, the maximum shear or reaction force on the middle joist alleviates to 1.70 kN, 1.35 kN, and 1.25 kN, respectively. The bending moment is calculated as 0.44 kN-m, 0.36 kN-m, and 0.33 kN-m, while the deflection comes out to be 0.07 mm, 0.06 mm, and 0.05 mm for the three angles. This subsequently allows using 2 × 4 wooden lumbers for 60° tilt design. For the remaining load scenarios, a 2 × 6" wooden member shall be used.

3.3.2. Wire Rope

To determine the load on the wire rope, consider a tributary width of 0.534 m to determine the uniformly distributed load (UDL) which comes out to be 2.03 kN/m using Equation (A15). For the cantilever design, a tributary width of 1.054 m is considered and UDL is found out to be 3.93 kN. The maximum shear or reaction comes out to be 2.14 kN and 2.05 kN at the ends following Equation (A16) shown in Figure 10.

To determine the load on the wire rope, a truss analysis is performed, detailed in Appendix C. The force on the wire cables connecting the modules from the top is considered only. This is to make the analysis conservative, where the snow, wind, and dead load act from the top. So, if the wires at the top survive, the bottom wires will perform satisfactorily as well. Furthermore, 2.15 kN force will be acting vertically downwards on each wire rope, as shown in Figure 7. The maximum tension in the wire rope comes out to be 8.30 kN. Similarly, for cantilever design, a 2.06 kN force acts vertically downwards on the cable which results in a maximum tension of 7.95 kN. The load is then transferred to the post.

Changing the angle of the wire cable reduces the force it experiences while holding the modules. For horizontal modules, changing the angle from 75° to 15° varies the force in the cable from 8.30 kN to 2.22 kN, respectively. A suitable cable can then be selected based on the system design and parameters. Similar to the two-module design, an iterative analysis for wire rope is performed for different angles. The calculations suggest that the cable experiences 7.95 kN force when installed at a 75° angle which reduces to 2.13 kN when the angle reduces to 15°. Figure 11 represents a graphical account of the analysis.

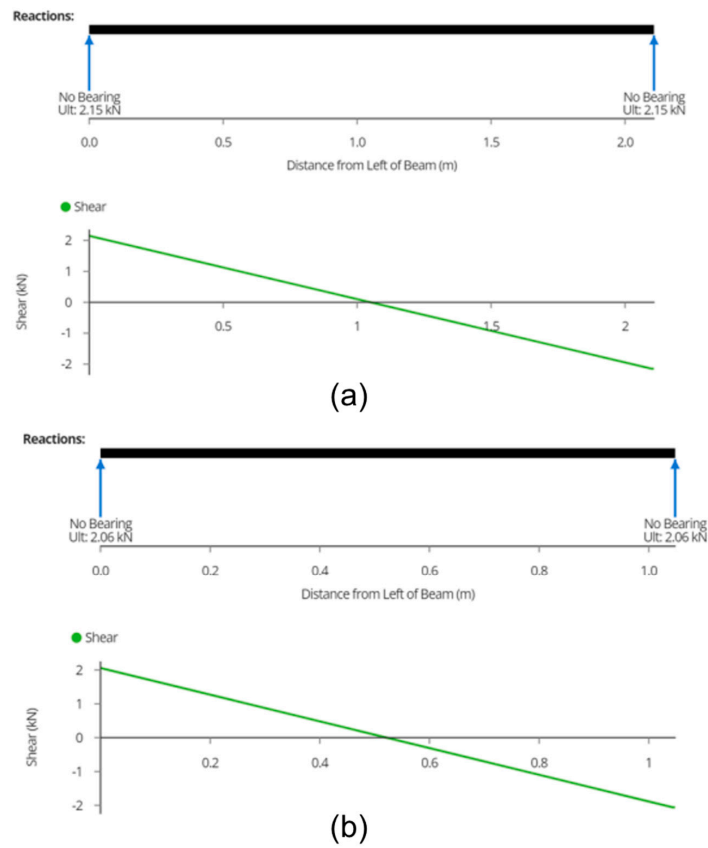


Figure 10. Reaction and Maximum Shear Forces (a) T-shaped design, (b) Cantilever designs (one and two module).

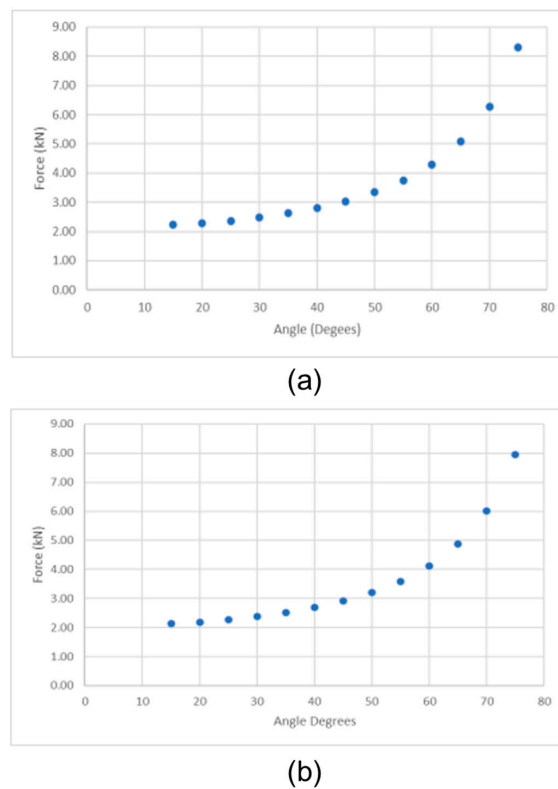


Figure 11. Graph of force experienced by wire cable at different angles for (a) two module design and (b) cantilever design.

3.3.3. Posts

The allowable force for a 6×6 column 1848 mm in height comes out to be 223.43 kN, while for an 8×8 column, it is calculated as 666.66 kN (Equation (A19)). From the truss analysis (details in Appendix C), the load acting on the posts is determined to be 8.16 kN (Figures 12 and 13).

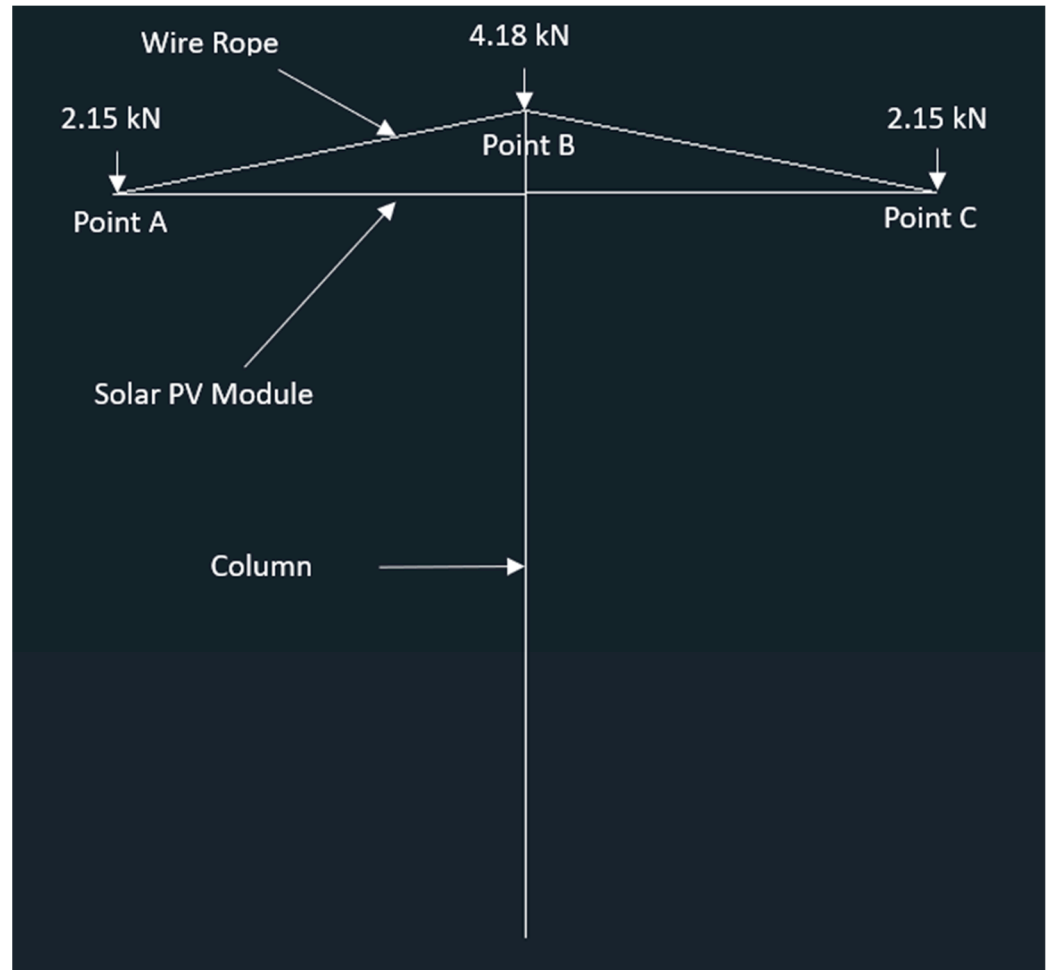


Figure 12. Truss analysis for the T-shaped two module racking structure.

Regarding the ground, if the applied pressure surpasses the permissible limit, there are two potential courses of action. Firstly, 150 mm of compacted clear stone gravel can be added to the base of the footing. Alternatively, the diameter of the footing can be increased.

Figure 14 shows the FEA results of the PV module under the proposed configuration and load combination of wind, snow, and dead load (3620 Pa). According to the FEA, the maximum stress on the PV module (129.80 MPa placed on the middle of frame’s width) is lower than strength of aluminum, proving the mechanical stability of PV module under this configuration. Furthermore, using this type of installation and load for PV modules will lead to the maximum displacement of 20.99 mm in the middle of PV module’s laminate. Comparing these values with similar studies in the literature [64] reveals that PV modules under the IEC 2400 Pa load exhibit the maximum stress from 78 MPa to 138 MPa and the maximum deflection from 9.2 mm up to 18.6 mm. Considering the fact that in this study, the net load of 3620 Pa is considered, results are in line with the literature results. Excluding the fixture from the bottom of the PV module can increase the stress and deflection of PV module, significantly leading to failure under the 3620 Pa load as shown in Figure 15. Therefore, using the fixture is crucial as a support provider for the bottom

of frame, preventing the maximum stress on the PV module to exceed the strength limit. Similarly, FEA results for side bolts model presented in Figure 16 demonstrate instability in this configuration, leading to exceeding the strength limit of aluminum considerably. Using this design in the real world, in the presence of extreme weather conditions, can lead to the failure of PV modules. Hence, modifications are needed for this design to make it mechanically stable, such as adding a fixture under the bottom of PV module as a support similar to what is presented in the main design.

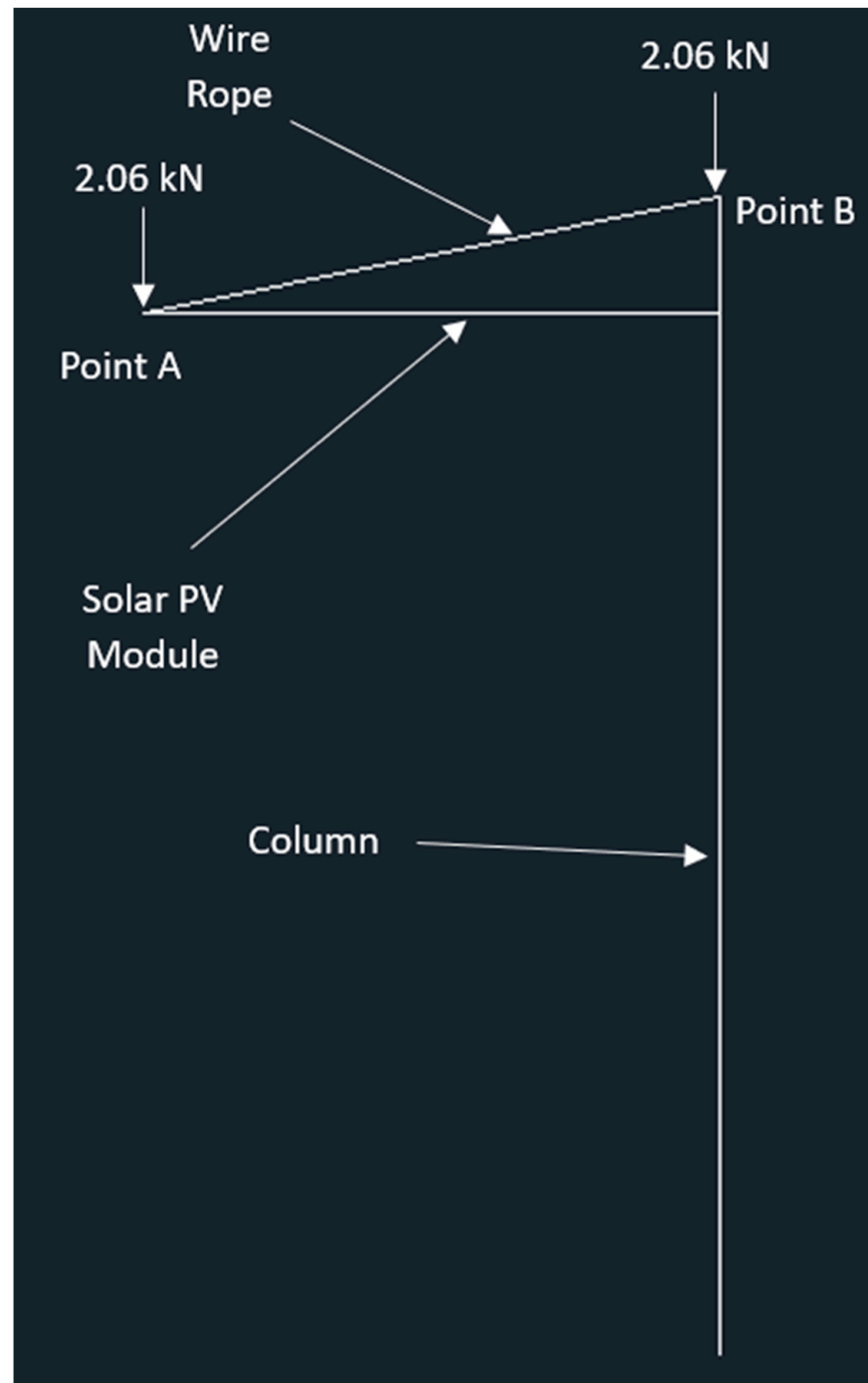


Figure 13. Truss analysis for the cantilever racking structure.

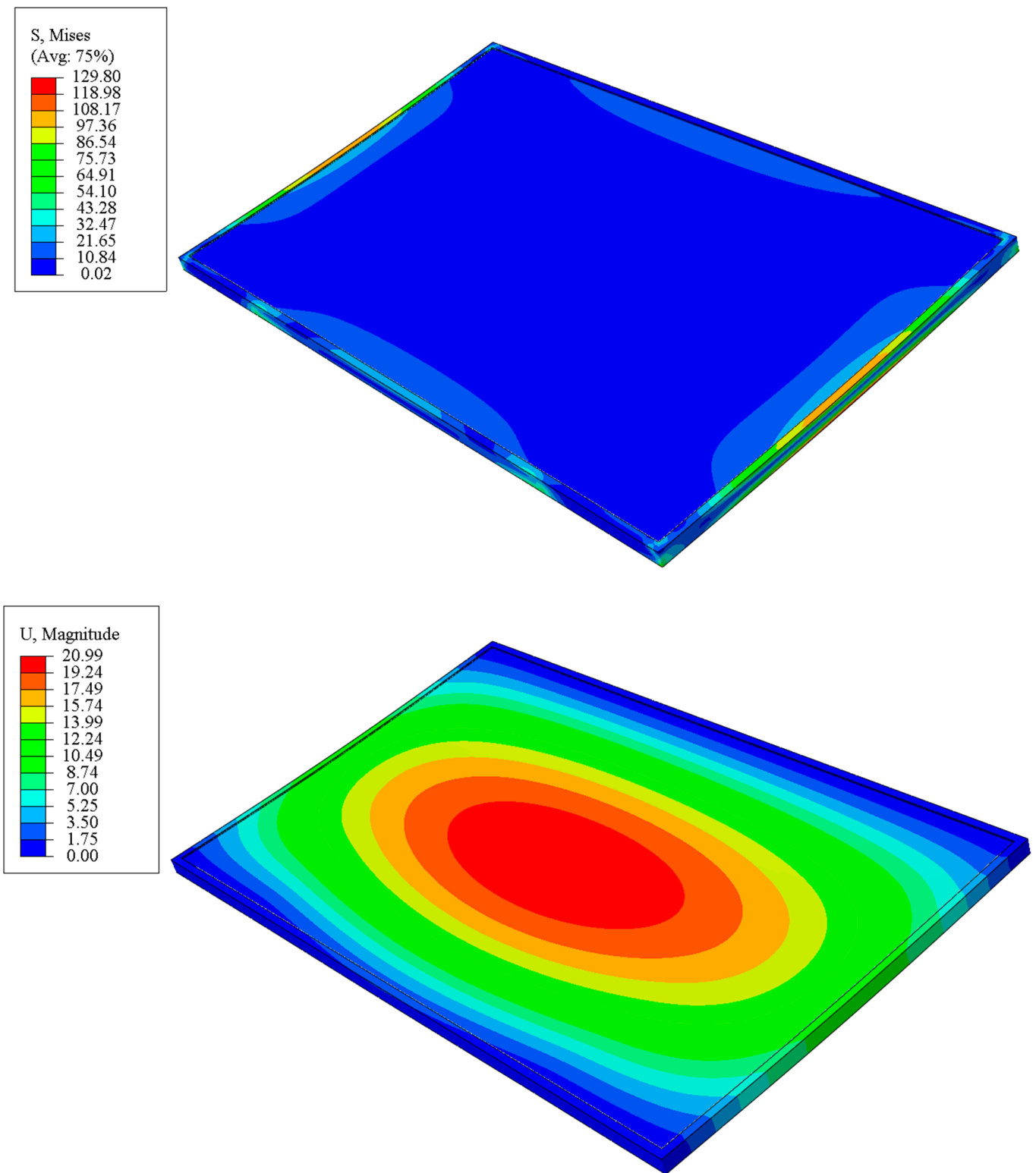


Figure 14. Stress in MPa (**top**) and displacement in mm (**bottom**) of PV module based on FEA results—Main proposed design.

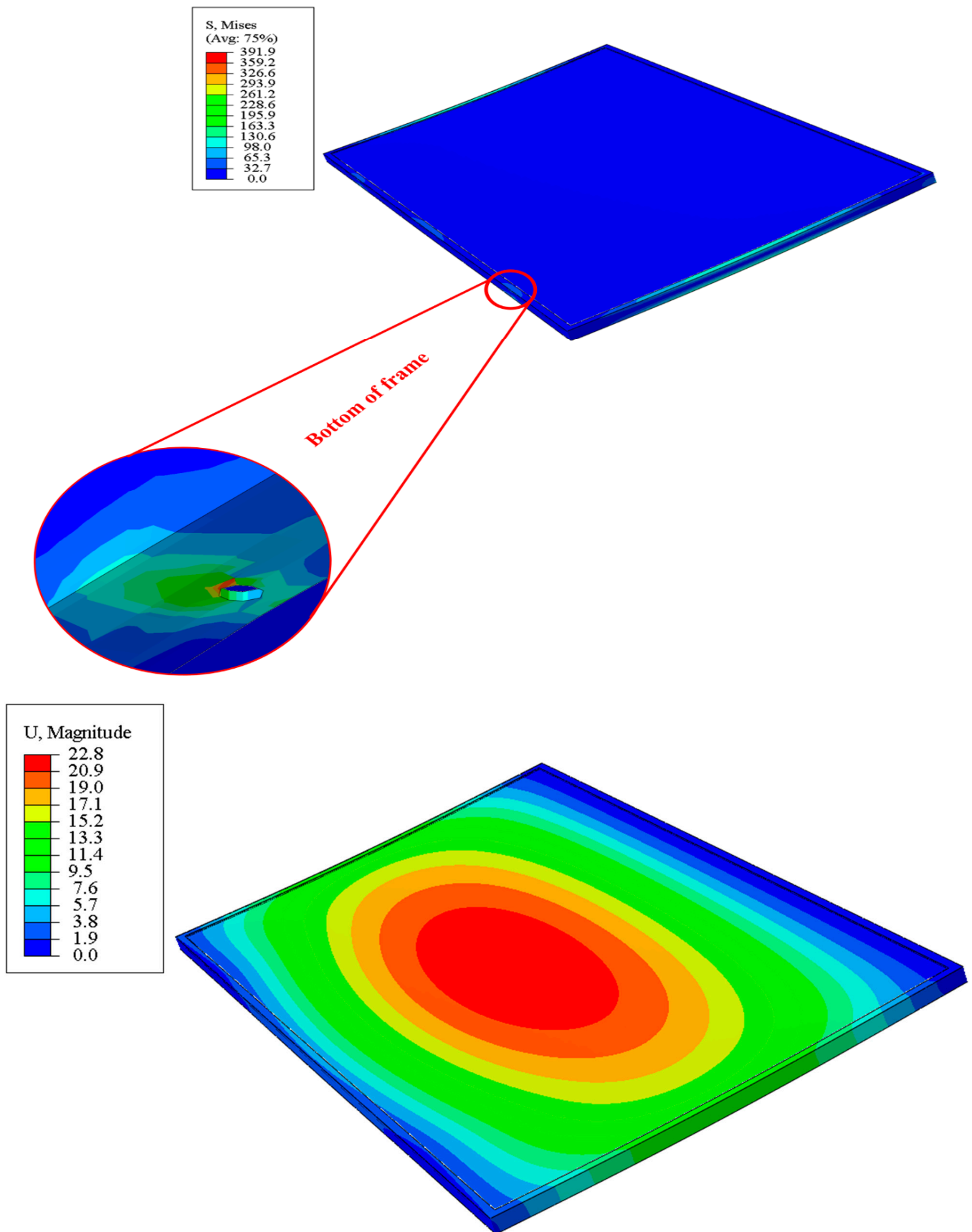


Figure 15. Stress in MPa (top) and displacement in mm (bottom) of PV module based on FEA results—Main design without fixture.

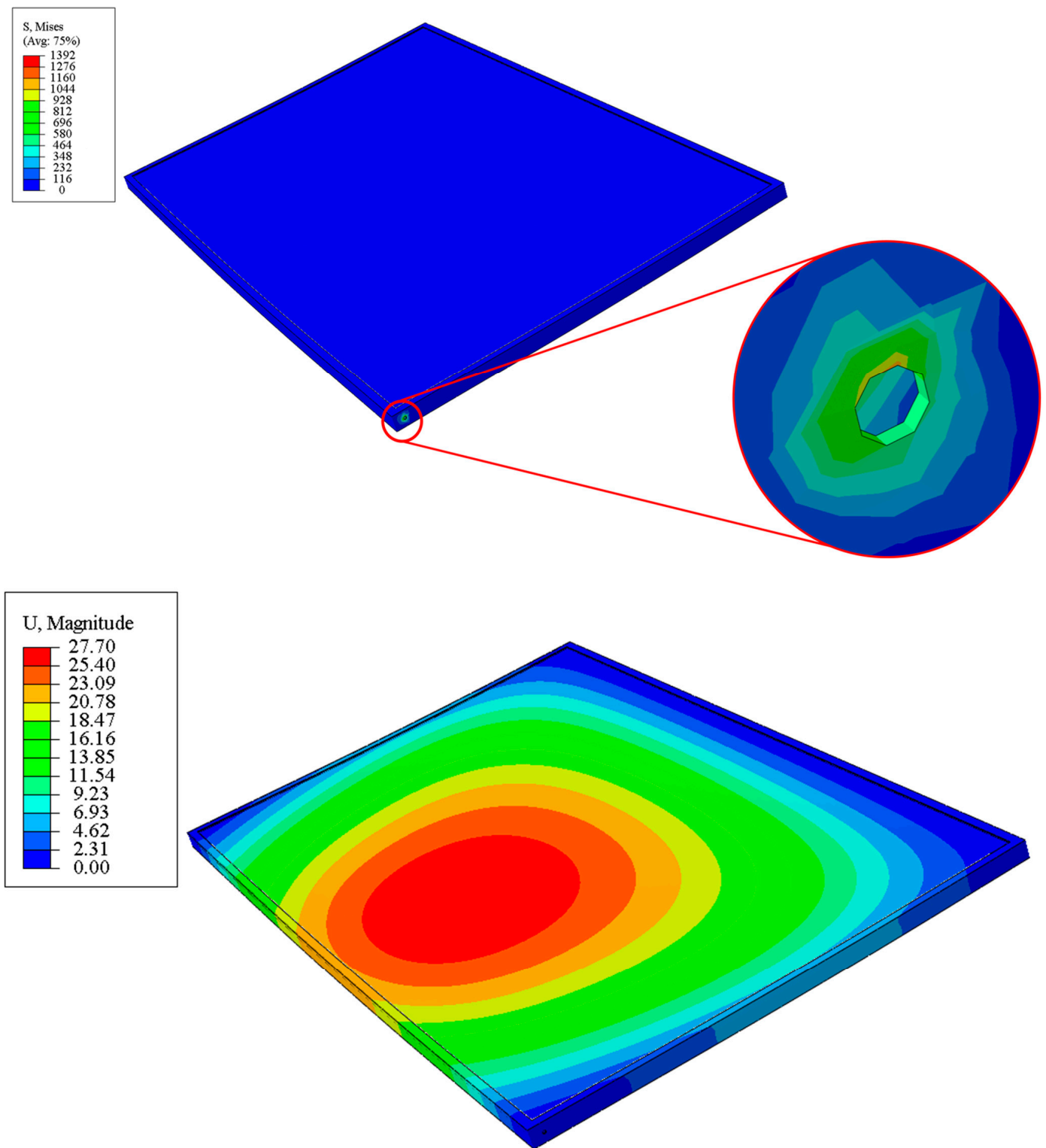


Figure 16. Stress in MPa (**top**) and displacement in mm (**bottom**) of PV module based on FEA results—Side bolts model.

The racking design is competitive when compared to other racking designs as shown in Table 12.

Table 12. Economic Analysis of Different Wood-based PV Racking Designs.

| Racking System | Cost (CAD) | Cost (CAD/Watt) |
|--|------------|-----------------|
| Fixed Racking Configuration [44] | 426 (389) | 0.35 (0.32) * |
| Variable Tilt Racking Configuration [45] | 438 (406) | 0.36 (0.34) * |
| Vertical Wood Racking Configuration [46] | 371 (300) | 0.15 (0.13) * |
| T-shaped Racking Configuration (2-module Design) | 397 | 0.43 |
| T-shaped Racking Configuration (4-module Design) | 1155 | 0.63 |
| Sloped Racking Configuration | 372 | 0.40 |
| Inverse Y Racking Configuration | 427 | 0.46 |
| Fixed Racking Configuration (Modified to 1.8 m with 6 × 6 columns) | 526 | 0.44 |
| Variable Tilt Racking Configuration (Modified to 1.8 m with 6 × 6 columns) | 598 | 0.50 |
| Cantilever Carport Racking Configuration (one module) | 471 | 1.00 |
| Cantilever Carport Racking Configuration (two modules) | 612 | 0.66 |
| Variable tilt Wood and Wire Rope T-shaped Configuration | 410 | 0.44 |

* Originally reported values in publications in brackets lower because of economic cost changes.

4. Discussion

4.1. Wooden Racking Economics

The levelized cost of electricity (LCOE) is an excellent measure to show the influence of transitioning from a fixed tilt racking design to a variable tilt racking configuration on energy production. Although the initial investment for a fixed tilt system may be lower, previous studies have indicated that the LCOE values for both the systems (fixed and variable tilt) come out to be similar (~CAD 0.01/kWh) [45]. This aspect plays a crucial role for the user/customer in determining which racking design was to be installed at the location. The designs presented in this study are suitable for installations at various locations and applications including carports, agricultural lands, etc.

These variable tilt racking structures using metal cables are cost effective when compared to the ones commercially available. The racking systems presented in this study also present similar functionality as those available in the market. Also, the racking design will require minimal labor to be set up and installed. The system does not require any cutting as the wooden members of the sizes mentioned in the BOM can be used. There are only two joists to column connections, while the remaining connections are made through cable clamps and eye hooks. The cost of typical ground mount commercial racking designs vary from USD 0.68/W (CAD 0.92/W) to USD 1.15/W (CAD 1.55/W) for a 1 kW solar PV system [69]. Previously presented wood racking designs cost from around CAD 0.13/W to CAD 0.50/W. These structures are generally fixed tilt; the only variable tilt design in the literature is a low height conventional racking system. The configurations presented here provide a stilt-mounted variable tilt racking, particularly useful to be used in carports and in any type of agrivoltaics systems where equipment or livestock needs to traverse underneath the modules. The carport racking designs commercially available range from CAD 1.30 to 1.50 per W [70]. According to Energy Sage, the average cost of a complete solar carport is USD 3.31/W, which is approximately 18% more expensive than a normal rooftop installation [71]. SunWatts offers carport racking designs (up to 16 kW rating) at a price of USD 1.56/W [72]. According to the NREL report in 2021, the racking cost for a residential PV system is USD 0.08/W, a commercial PV system is USD 0.11–0.17/W, while for a large scale solar farm, it is USD 0.12/W [73]. The racking configuration discussed in this article can also be employed on pathways or walkway awnings. The integration would certainly be beneficial as an energy generation source but it might also give an aesthetic appeal to the structure while at the same time provide shelter. Using semi-transparent PVs that allow diffused sunlight to pass through may further create a visually captivating ambiance with novel racking structure.

For proof-of-concept, an agrivoltaic system was built with spectral-shifting semi-transparent PV modules as shown in Figure 17. Turnbuckles and hooks are used at one end of the cable (where it attaches with 6 × 6 column) while eyebolts are used at the other end. An angle iron is attached to the solar modules to connect the eyebolts. Two light duty T-hinges (Figure 18) are used for changing the tilt of the module as the turnbuckle is loosened/tightened; moreover, different lengths of cables can also be used to change the tilt angle of the solar modules.



(a)

Figure 17. Cont.



(b)



(c)

Figure 17. Proof-of-concept Build of Wire-rope racking design: (a)70-degree tilt, (b) 45-degree tilt, and (c) 0°-degree tilt.



Figure 18. Hinge for changing the tilt angle of the module.

4.2. Agrivoltaics

There is a growing concern among rural residents about large scale PV developments, similar to what has been observed in conflicts over wind power siting [74,75]. The resistance to large-scale PV deployment mainly arises from worries about reduced agricultural productivity and subsequent employment impacts and potential food insecurity/raises in food costs [76–79]. Thankfully, this conflict can be resolved by employing a dual land use approach, allowing land to be utilized for both solar PV electricity generation and farming, a concept known as agrivoltaics [32–35,37].

Agrivoltaics offer a wide range of benefits, including renewable electricity generation, reduced greenhouse gas emissions, enhanced crop yields, protection of plants from excessive solar energy and inclement weather conditions, such as hail, etc., water conservation, agricultural employment, local food production, and increased revenue [80]. The variable tilt stilt-mounted racking systems analyzed in this study holds particular value for agrivoltaics. The designs offer a very cost-effective solution tailored for agrivoltaic farms. The modules are elevated to allow ease of agricultural operations including harvesting, planting, or weeding. Crops including cucumbers, grapes, kiwi, melons, peas, passion fruit, pole beans, pumpkins, strawberries, squash, tomatoes, etc., are well suited for this racking configuration [49,81]. The tilt angle for solar modules can also be altered for plant protection [81]. The adjustment of tilt angle requires minimal labor by using one of two approaches. If the tilt angle adjustment is modest, then turning the turnbuckles will result in a change of the tilt. If a large adjustment is needed in the tilt angle, then different lengths of cables can be substituted for the cable lengths shown here to enable the change of tilt to

be whatever angle is required over the entire range. The combination of farming and PV electricity generation provides a dual revenue stream for farmers increasing profits per acre. Deployment of agrivoltaics can also enhance the stability of rural electric grids. Finally, if agrivoltaic systems incorporate storage, they can create emergency islanded power grids to reduce outage impacts, a valuable feature for isolated communities [82,83]. The market for agrivoltaics is expected to increase exponentially in the coming years. It is projected to expand from USD 4.1 billion in 2023 to USD 8.9 billion in 2030 [30]. It has already surpassed USD 3.5 billion in 2022 [30].

4.3. Wood Price Sensitivity

The system’s cost is significantly influenced by fluctuations in lumber prices. Record volatility was observed in wood prices in 2021 [84]. The contract lumber’s commodity price index chart, depicting the average rough framing lumber package, is a tool that assists keeping track of the percentage increase/decrease in price over time [84]. In 2020, the price index was 70% higher than 2019, while the first six months of 2021 showed 108% increase [84]. When compared to 2015, the price of wood increased at least two-fold as of 2021 [85]. Price volatility in wood products is mainly driven from conservatism, lack of infrastructure, and emotional trading [86]. The expenses associated with this design will also depend on the accessibility of the local wood market and, if imported, the applicable taxes and import duties. Table 13 provides information about the standard prices of construction-grade pressure-treated 2 × 4 × 8 lumber in different countries. A previous study have revealed that wood-based racks were more cost-effective in North America and certain South American nations, whereas metal proved to be a more economical choice in Central and South America [55].

Table 13. Difference in wood prices in different parts of the world.

| Country | Price [CAD] ¹ | Source ² |
|----------------|--------------------------|--|
| Canada | 7.69 | The Home Depot, London, Canada |
| USA | 6.62 | The Home Depot, Detroit, USA |
| United Kingdom | 5.84 | B&Q, London, UK |
| Netherlands | 16.04 | Woodvision, Kampen, The Netherlands |
| Australia | 13.29 | Australian Treated Pine Pty Ltd., Melbourne, Australia |
| Brazil | 12.13 | Fremade Madeiras, São Paulo, Brazil |
| India | 12.45 | IndiaMart, Uttar Pradesh, India |

¹ Priced as of 1 November 2023. ² Prices at each source’s competition are approximately the same.

This is the first open-source wood-based photovoltaic racking that allows variation in the tilt angle for a stilt-mounted structure. The designs offer several distinct attributes. First, it is constructed from sustainable, locally available materials, thus promoting environmental responsibility. Second, the design process is simple, only requiring very few fabrication/construction steps. It can therefore be easily manufactured using basic hand tools, making it accessible to an average user. Moreover, it aligns with the industry standard PV warranty by providing a 25-year lifespan. The racking configuration is robust and resilient as it can withstand high windspeeds and significant snow loads, adapting to specific regional conditions. Furthermore, it is cost-effective, making it an economical choice. Lastly, it operates under an open-source license, facilitating widespread access for self-fabrication and allowing companies to create customized versions for local markets.

4.4. Permits and Certification

Although roof-mounted PV systems require professional engineering stamps and building permits to install, these ground-mounted systems do not require these. Racking only requires a professional engineer’s stamp of approval if the racking is not CSA approved [87]. In the case of this system, all wood used is marked and graded as SPF No.2 grade, which indicates CSA’s approval for structural use. The design complies with

National Research Council's National Building Code of Canada, which works together with CSA, and the National Design Specification for Wood Construction, which follows CSA O86:19 Engineering design in wood.

Most municipalities, such as the City of Toronto, do not require building permits for ground-mounted PV systems of any size, and thus plans and calculations do not need to be stamped and signed by a registered engineer [88]. Some municipalities, such as the City of Waterloo, specify that building permits are not required such that the system is not connected to water or heating resources [89]. Very few municipalities, such as the city of London, only require a work permit if excavation is required, or if scaffolding and cranes are used [90]. In all cases, these ground-mounted systems are an exceptional alternative to roof-mounted systems because they avoid a lot of the red-tape associated with an existing structure. This allows costs to remain low, construction to be completed quickly, and for PV systems to remain a feasible option as a DIY alternative.

4.5. Future Work

The racking designs presented in the paper have the potential for further research and innovation. Although the system integrates clean energy generation with sustainable construction material (wood), an investigation needs to be undertaken looking into advanced sustainable composite materials which are more resilient, weather resistant, and provide a longer lifespan. More efficient and cost-effective designs for PV racking need to be further explored. This can be done by optimizing manufacturing processes, reducing installation costs, and increasing market awareness. Structural design optimization is key to further integrate PV technology in the communities. Furthermore, a comprehensive life cycle analysis (LCA) assessing the environmental impacts of wood-based PV racking systems similar to those generally conducted on PV should also be performed [91,92]. An overall evaluation of carbon footprint and energy requirements of these designs compared to others can be made part of such a study. Research focusing on understanding the maintenance and durability of these racking designs should also be carried out and compared to those of the overall system [93,94]. This may include a monitoring system for the detection of issues and periodic replacement of deteriorated wooden members. Another important aspect to be looked at includes the development of guidelines, procedures, and standards for the responsible sourcing of wood, which is utilized in the renewable energy industry. Moreover, innovative techniques to preserve wood which can improve decay resistance properties of wood can also be explored.

5. Conclusions

This study outlined two novel open-source wood- and cable-based PV racking systems with adjustable tilt angles that exceed Canadian building code standards and are thus applicable to most of the world's populations. These are the first stilt-mounted solar photovoltaic racking designs that allow change of tilt angle by varying the length of cables. The tilt angle can vary from 0° (horizontal) to 90° (vertical), thus offering a distinct feature and flexibility not explored in the previous literature. The systems offer significant economic savings and incur from approximately one-third to less than two-thirds of the capital expenses of the commercially available variable tilt racking solutions. In addition, the racking designs are easy-to-build and require minimal manufacturing operations. These features indicate that they would be widely accessible throughout the world. The economic analysis indicates that, in various scenarios, the new variable tilt rack offers the most cost-effective option, but these results are heavily material, labor, and location dependent. Ultimately, the innovative design of the variable tilt racking system presented here has several distinct advantages over fixed tilt designs, especially in applications like agrivoltaics. The stilt-mounted designs can be employed for agrivoltaic settings since the solar modules are installed at increased height than conventional PV racking structures and thus allow farm workers shaded ergonomic access to perform planting, weeding, and harvesting operations. Future work is needed to determine the life cycle analysis of this system including the results of long-term outdoor field trials.

Author Contributions: Conceptualization, J.M.P.; methodology, U.J. and N.V.; software, U.J., S.A.S. and N.V.; validation, U.J., S.A.S. and N.V.; formal analysis, U.J., N.V., S.A.S. and J.M.P.; investigation, U.J., S.A.S. and N.V.; resources, J.M.P.; data curation, U.J. and N.V.; writing—original draft preparation U.J., N.V. and J.M.P.; writing—review and editing, U.J., N.V., S.A.S. and J.M.P.; visualization, U.J., S.A.S. and N.V.; supervision, J.M.P.; funding acquisition, J.M.P. All authors have read and agreed to the published version of the manuscript.

Funding: This research was funded by Thompson Endowment and the Natural Sciences and Engineering Research Council of Canada (NSERC).

Data Availability Statement: Data will be made available upon request.

Conflicts of Interest: The authors declare no conflict of interest. The funders had no role in the design of the study; in the collection, analyses, or interpretation of data; in the writing of the manuscript, or in the decision to publish the results.

Appendix A. Design Analysis Assumptions

Here, several assumptions have been made to streamline the calculations, and they have been deliberately kept conservative to ensure structural integrity under the most extreme field conditions. To elaborate:

All applied loads are considered to act perpendicular to the module face, ensuring that the middle joist undergoes the maximum flexural load.

All members are connected with pins and have no fixed end moments. This assumption takes into account that joist hangers and brackets allow for rotation [95].

Following NBCC 4.1.6, the wind and snow load are assumed to be evenly distributed across the module surface, as considerations for snow and wind accumulation apply primarily to large structures [96].

The Heliene 144HC M6 module is specified to withstand a front load of up to 5400 Pa and a rear load of up to 2400 Pa [57]. Given that the design loads will be significantly lower than these values, the modules exhibit ample structural capacity.

Appendix B. Load Calculations

Appendix B.1. Snow Loads

The specified snow load is determined as per National Building Code of Canada (NBCC) [96]:

$$S = I_s [S_s (C_b C_w C_s C_a) + S_r] \text{ [kPa]} \quad (A1)$$

The importance factor for snow load (I_s) is considered as 1.15 since the failure of PV racking structure poses a risk to the life of people working underneath the structure. This is a conservative estimate as a factor of 1.00 could be used since the risk of people being under the racks in inclement weather, such as high winds and storms, is very low.

The 1-in-50-year ground snow load factor (S_s) is dependent on the location where the racking structure is being built. Using Table C-2 in NBCC for London, ON, a value of 1.90 is determined.

The basic roof snow load factor (C_b) is considered 0.80 if l_c is less than or equal to the factor $(70/C_w^2)$. Here, C_w is the wind exposure factor and l_c is the characteristic length of the upper or lower roof. The value of l_c is evaluated using the Equation $2w - w^2/1$ where w is the smaller plan dimension of the roof and l is the larger plan dimension of the roof. For the design, l_c is found out to be less than $(70/C_w^2)$.

The wind exposure factor (C_w) is considered as 0.75 since our racking design will be exposed to wind in all directions.

The slope factor (C_s) is dependent on the tilt angle of the system. Assuming the slope is less than 15° , C_s is taken as 1.

For calculations, the accumulation factor (C_a) is considered 1.00 for small single slope structures.

The 1-in-50-year associated rain load (S_r) is dependent on the location where the racking structure is built. Following Table C-2 of NBCC for London, ON, a value of 0.4 is ascertained.

Table A1 summarizes the factors used for calculating snow load.

Table A1. Snow Load Factors.

| Factor | Value |
|---------------------------------------|------------------------|
| Importance Factor (I_s) | 1.15 |
| Snow Load Factor (S_s) | 1.90 |
| Basic Roof Snow Load Factor (C_b) | 0.80 |
| Wind Exposure Factor (C_w) | 0.75 |
| Slope Factor (C_s) | 1.00, 0.67, 0.33 and 0 |
| Accumulation Factor (C_a) | 1.00 |
| Associated Rain Load (S_r) | 0.40 |

Appendix B.2. Wind Load

Using National Building Code of Canada (NBCC) 2020, the wind load is determined, which is a summation of both external wind pressure as well as internal wind pressure.

$$W = p + p_i \text{ [kPa]} \tag{A2}$$

where W is the total wind load in kPa;

p is the specified external wind pressure in kPa;

p_i is the specified internal wind pressure in kPa.

The following equations govern the external and internal wind pressures:

$$p = I_w q C_e C_t C_p C_g \text{ [kPa]} \tag{A3}$$

$$p_i = I_w q C_{ei} C_t C_{gi} C_{pi} \text{ [kPa]} \tag{A4}$$

The wind importance factor (I_w) is considered 1.15 as the failure of PV rack may risk the life of people working underneath the structure.

The reference velocity pressure (q) is dependent on the location where the racking structure is constructed. Following Table C-2 in NBCC for London, ON, a value of 0.47 is ascertained.

The exposure factor (C_e) is calculated using the expression $(h/10)^{0.2}$. Here, h is considered 6 m as the height of the structure is less than 20 m while it is also less than the smaller plan dimension. The value of C_e is determined to be 0.90.

The topographic factor (C_t) is considered as 1.00.

The external pressure coefficient (C_p) and gust effect factor (C_g) are combined. Using Table 4.1.7.6, the value of the product is found to be -1.30 .

The exposure factor for internal pressure (C_{ei}) is the same as the exposure factor ' C_e ' since wind can attack the inside of the system in the same way as the outside.

The internal gust effect factor (C_{gi}) is taken as 2.00.

The internal pressure coefficient (C_{pi}) is taken as -0.70 .

Table A2 summarizes the factors used for calculating snow load.

Table A2. Wind load Factors.

| Factor | Value |
|--|---------|
| Wind Importance Factor (I_w) | 1.15 |
| Reference Velocity Pressure (q) | 0.47 |
| Exposure Factor (C_e) | 0.90 |
| Topographic Factor (C_t) | 1.00 |
| External Pressure Coefficient and Gust Effect Factor ' $C_p.C_g$ ' | -2.00 |
| Exposure Factor for Internal Pressure (C_{ei}) | 0.90 |
| Internal Gust Effect Factor (C_{gi}) | 2.00 |
| Internal Pressure Coefficient (C_{pi}) | -0.70 |

Appendix B.3. Dead Load

The structure's dead load 'D' takes into account the PV module weight and the wooden member weights and represents the weight of the structure itself. The weight of brackets and fasteners is insignificant compared to the design load and can be considered negligible.

Appendix B.4. Load Combinations

To address the simplified assumptions made during the design, it becomes imperative to include safety factors to the specified loads, aiming to minimize the probability of failure. These adjusted loads (factored loads) are combined as principal loads and companion loads, adhering to the load combinations outlined in Section 4.1.3.2 of NBCC. The calculations must carefully consider the combination of principal loads and companion loads that yield the highest net load. Principal loads constitute the essential loads requiring evaluation, while companion loads are incorporated only if they act in the same direction as the principal loads. It is crucial to highlight that the design wind load operates in the negative direction, whereas the governing snow load is in the positive direction. Consequently, combining these loads would reduce the net load and is therefore not recommended.

Appendix B.5. Wooden Members Structural Capacity

The National Design Specification for Wood Construction [68] provides reliable design values for a variety of wood types.

Although these capacities have shown reliability, it is extremely important to incorporate resistance factors into these capacities to accommodate unforeseen vulnerabilities and ensure an optimum, safe, and functional design.

The load duration factor (C_D) is taken as 1.15 considering typical design load, i.e., the governing load, as snow load.

The temperature factor (C_T) is considered 1.00 since the racking structure is not expected to be exposed to a temperature of above 100° F.

The wet service factor (C_M) is found to be 1.00 for calculating factor f_b , f_c , and f_t , 0.97 for factored f_v , and 0.90 for factored E and E_{min} .

The beam stability factor (C_L) is calculated as 0.64, 0.76, 0.97, and 0.98 according to the guidelines in Section 3.3.3 of National Design Specification [68].

The flat use factor (C_{fu}) is considered as 1.20 and 1.15 as per Table 4B of NDS Supplement [68].

The incising factor (C_i) is ascertained from Table 4.3.8 of NDS and comes out to be 0.8, except for when determining factored E and E_{min} , where its value is considered 0.95, and for f_c , where its value is considered as 1 [68].

The repetitive member factor (C_r) is taken as 1.00.

The size factor (C_F) is 1.10 as per Table 4A of NDS Supplement.

The compression factor (C_P) (calculated using the dimensions of the posts) is calculated in accordance with Section 3.7.1 of NDS and comes out to be 0.29 for 6 × 6 members.

The National Design Specifications for Wood Construction provide the formulae for calculating the factored properties. The formulae are given below:

$$\text{Factored bending stress} = f_b^* = f_b C_D C_M C_t C_L C_F C_{fu} C_i C_r \text{ [MPa]} \quad (A5)$$

$$\text{Factored shear stress} = f_v^* = f_v C_D C_M C_t C_i \text{ [MPa]} \quad (A6)$$

$$\text{Factored tensile stress} = f_t^* = f_t C_D C_M C_t C_F C_i \text{ [MPa]} \quad (A7)$$

$$\text{Factored compressive stress} = f_c^* = f_c C_D C_M C_t C_F C_i C_P \text{ [MPa]} \quad (A8)$$

$$\text{Factored Elastic modulus} = E^* = E C_M C_t C_i \text{ [MPa]} \quad (A9)$$

$$\text{Factored } E_{min} = E_{min}^* = E_{min} C_M C_t C_i C_T \text{ [MPa]} \quad (A10)$$

Using the factored capacities calculated equations described above and the dimensional properties of the wooden members, the resistance values are finally ascertained. The formulae are given below:

$$\text{Resisting bending moment} = M_r = (2f_b \cdot I/h) \text{ [kN-m]} \tag{A11}$$

$$\text{Resisting shear force} = V_r = (f_v \cdot I_b/Q) \text{ [kN]} \tag{A12}$$

$$\text{Resisting tensile force} = T_r = f_t \cdot A \text{ [kN]} \tag{A13}$$

$$\text{Resisting compressive force} = C_r = f_c \cdot A \text{ [kN]} \tag{A14}$$

To ensure the structural integrity of each member and circumvent system failure, the following conditions must be satisfied:

The resisting bending moment (M_r) must equal or exceed the maximum applied bending moment (M_{max}).

The resisting shear force (V_r) must equal or exceed the maximum applied shear force (V_{max}).

The resisting tensile force (T_r) must equal or exceed the maximum applied tensile force (T_{max}).

The resisting compressive force (C_r) must equal or exceed the maximum applied compressive force (C_{max}).

Additionally, the maximum deflection (D_{max}) should not surpass the member length divided by 360, adhering to NBCC 9.4.3.

Appendix B.6. Structural Analysis for T-Shaped Racking

The net load is evenly distributed across the module's dimensions. As specified by modules' supplier Heliene, the panels exhibit sufficient capacity to withstand these loads. Subsequently, the load is transferred from the panels to the joist and then the wire rope. The joist bears its own weight in the form of a uniformly distributed load, designated as 'w'.

$$W = 1.25 (OW) \text{ [kN]} \tag{A15}$$

OW is the own weight of the member. The load is multiplied by a factor of 1.25 since it is a dead load [97]. Moreover, to ascertain the uniformly distributed design load, the design load is multiplied with the tributary width for the joist under consideration. Total uniformly distributed load (UDL) is the sum of the own weight and design load.

The wood and cable design only uses one joist. A wooden plank with dimensions of $2 \times 12 \times 8'$ is considered for T-shaped variable tilt racking design and $2 \times 6 \times 8'$ is considered for cantilever racking configuration while 6×6 column is used for the posts for each design. In case the applied values of bending moment, shear, compression, tension, and deflection exceed the resistance values, a larger member should be evaluated.

The following formula is used to calculate the maximum shear force or the reaction for the middle joist:

$$\text{Maximum shear or reaction} = \text{Total UDL} \cdot L/2 \text{ [kN]} \tag{A16}$$

where L is the length of the joist.

The maximum bending moment is ascertain using the following equation:

$$\text{Maximum moment} = \text{Total UDL} \cdot L^2/8 \text{ [kN-m]} \tag{A17}$$

The maximum deflection in the member is ascertained from the following formula:

$$\text{Maximum deflection} = 5 \cdot \text{Total UDL} \cdot L^4/384EI \text{ [mm]} \tag{A18}$$

Analysis for the joist and wire rope is also performed using Clearcals.

Subsequently, the buckling check for the posts is performed using the Euler Buckling equation given below:

$$C_{\text{buckling}} = \pi^2 EI_{\text{weak}} / (Lk)^2 \text{ [MPa]} \tag{A19}$$

where the effective length factor, k , is considered two for a column fixed at its base, and free on the opposite end. Next, wire rope and the column are considered to be a truss structure and a truss analysis is performed to determine the forces. The reaction forces from the joist and solar module are considered the applied forces acting on the truss.

Appendix C. Truss Analysis

Appendix C.1. Calculations for 2-Panel T-Shaped Design

Appendix C.1.1. Point A

Using summation of forces as 0 across point A; the forces acting along the member F_{AB} and F_{AB} is determined.

$$\begin{aligned}\Sigma F_y &= 0 \\ -2.14 + F_{AB}\cos(75) &= 0 \\ F_{AB} &= 8.30 \text{ kN}\end{aligned}\tag{A20}$$

Appendix C.1.2. Point B

$$\begin{aligned}\Sigma F_y &= 0 \\ 2F_{AB}\cos(75) + 4.18 &= F_{COL} \\ F_{COL} &= 8.48 \text{ kN}\end{aligned}\tag{A21}$$

Appendix C.2. Calculations for Cantilever Carport Design

Appendix C.2.1. Point A

Using summation of forces as 0 across point A; the forces acting along the member F_{AB} and F_{AB} is determined.

$$\begin{aligned}\Sigma F_y &= 0 \\ -2.06 + F_{AB}\cos(75) &= 0 \\ F_{AB} &= 7.95 \text{ kN}\end{aligned}\tag{A22}$$

Appendix C.2.2. Point B

$$\begin{aligned}\Sigma F_y &= 0 \\ 2F_{AB}\cos(75) + 2.06 &= F_{COL} \\ F_{COL} &= 6.18 \text{ kN}\end{aligned}\tag{A23}$$

References

- Lu, Y.; Yi, F.; Yu, S.; Feng, Y.; Wang, Y. Pathways to Sustainable Deployment of Solar Photovoltaic Policies in 20 Leading Countries Using a Qualitative Comparative Analysis. *Sustainability* **2022**, *14*, 5858. [CrossRef]
- Fu, R.; Feldman, D.J.; Margolis, R.M. *US Solar Photovoltaic System Cost Benchmark: Q1 2018*; National Renewable Energy Lab. (NREL): Golden, CO, USA, 2018.
- Matasci, S. Solar Panel Cost: Avg. Solar Panel Prices by State in 2019: EnergySage. *Sol. News EnergySage* **2019**, *5*. Available online: <https://www.energysage.com/local-data/solar-panel-cost/> (accessed on 18 October 2023).
- Tsuma, M.; Kibaara, S. A Review of Levelized Cost of Electricity for Photovoltaic Systems Combining with Their Environmental Impacts. In Proceedings of the Sustainable Research and Innovation Conference, Juja, Kenya, 12 November 2022; College of Engineering and Technology at Jomo Kenyatta University of Agriculture and Technology. pp. 220–225.
- Dudley, D. Renewable Energy Will Be Consistently Cheaper Than Fossil Fuels By 2020. *Forbes* **2019**. Available online: <https://www.forbes.com/sites/dominicdudley/2018/01/13/renewable-energy-cost-effective-fossil-fuels-2020/?sh=189264e74ff2> (accessed on 18 October 2023).
- Solar Industry Research Data. Available online: <https://www.seia.org/solar-industry-research-data> (accessed on 18 October 2023).
- Vaughan, A. Time to Shine: Solar Power Is Fastest-Growing Source of New Energy. *Guardian* **2017**, *4*. Available online: <https://www.theguardian.com/environment/2017/oct/04/solar-power-renewables-international-energy-agency> (accessed on 18 October 2023).
- Barbose, G.L.; Darghouth, N.R.; LaCommare, K.H.; Millstein, D.; Rand, J. *Tracking the Sun: Installed Price Trends for Distributed Photovoltaic Systems in the United States-2018 Edition 2018*; Lawrence Berkeley National Lab. (LBNL): Berkeley, CA, USA, 2018.
- IEA Solar PV—Renewables 2020—Analysis. Available online: <https://www.iea.org/reports/renewables-2020/solar-pv> (accessed on 18 October 2023).

10. Levin, T.; Thomas, V.M. Can Developing Countries Leapfrog the Centralized Electrification Paradigm? *Energy Sustain. Dev.* **2016**, *31*, 97–107. [[CrossRef](#)]
11. Lang, T.; Ammann, D.; Girod, B. Profitability in Absence of Subsidies: A Techno-Economic Analysis of Rooftop Photovoltaic Self-Consumption in Residential and Commercial Buildings. *Renew. Energy* **2016**, *87*, 77–87. [[CrossRef](#)]
12. Hayibo, K.S.; Pearce, J.M. A Review of the Value of Solar Methodology with a Case Study of the U.S. VOS. *Renew. Sustain. Energy Rev.* **2021**, *137*, 110599. [[CrossRef](#)]
13. Pitt, D.; Michaud, G. Assessing the Value of Distributed Solar Energy Generation. *Curr. Sustain. Renew. Energy Rep.* **2015**, *2*, 105–113. [[CrossRef](#)]
14. Agenbroad, J.; Carlin, K.; Ernst, K.; Doig, S. *Minigrids in the Money: Six Ways to Reduce Minigrad Costs by 60% for Rural Electrification*; Rocky Mountain Institute: Basalt, CO, USA, 2018.
15. Szabó, S.; Pinedo Pascua, I.; Puig, D.; Moner-Girona, M.; Negre, M.; Huld, T.; Mulugetta, Y.; Kougiyas, I.; Szabó, L.; Kammen, D. Mapping of Affordability Levels for Photovoltaic-Based Electricity Generation in the Solar Belt of Sub-Saharan Africa, East Asia and South Asia. *Sci. Rep.* **2021**, *11*, 3226. [[CrossRef](#)]
16. Awan, A.B. Optimization and Techno-Economic Assessment of Rooftop Photovoltaic System. *J. Renew. Sustain. Energy* **2019**, *11*, 033501. [[CrossRef](#)]
17. Wang, P.; Yu, P.; Huang, L.; Zhang, Y. An Integrated Technical, Economic, and Environmental Framework for Evaluating the Rooftop Photovoltaic Potential of Old Residential Buildings. *J. Environ. Manag.* **2022**, *317*, 115296. [[CrossRef](#)]
18. Renewables International, 2013. Photovoltaics after Grid Parity Plug-and-Play PV: The Controversy 2013. Renewables 2013. Available online: <http://www.renewablesinternational.net/plug-and-play-pv-the-controversy/150/452/72715/> (accessed on 18 October 2023).
19. Barbose, G.; Darghouth, N.; Millstein, D.; Cates, S.; DiSanti, N.; Widiss, R. *Tracking the Sun IX: The Installed Price of Residential and Non-Residential Photovoltaic Systems in the United States*; LBL Publications: Berkeley, CA, USA, 2016. Available online: <https://escholarship.org/uc/item/9s90c8c6> (accessed on 18 October 2023).
20. Khan, M.T.A.; Norris, G.; Chattopadhyay, R.; Husain, I.; Bhattacharya, S. Autoinspection and Permitting With a PV Utility Interface (PUI) for Residential Plug-and-Play Solar Photovoltaic Unit. *IEEE Trans. Ind. Appl.* **2017**, *53*, 1337–1346. [[CrossRef](#)]
21. Khan, M.T.A.; Husain, I.; Lubkeman, D. Power Electronic Components and System Installation for Plug-and-Play Residential Solar PV. In Proceedings of the 2014 IEEE Energy Conversion Congress and Exposition, ECCE, Pittsburgh, PA, USA, 14–18 September 2014; pp. 3272–3278.
22. Lundstrom, B.R. *Plug and Play Solar Power: Simplifying the Integration of Solar Energy in Hybrid Applications*; Cooperative Research and Development Final Report. CRADA Number CRD-13-523; National Renewable Energy Lab. (NREL): Golden, CO, USA, 2017.
23. Mundada, A.S.; Prehoda, E.W.; Pearce, J.M. U.S. market for solar photovoltaic plug-and-play systems. *Renew. Energy* **2017**, *103*, 255–264. [[CrossRef](#)]
24. Fthenakis, V.; Alsema, E. Photovoltaics Energy Payback Times, Greenhouse Gas Emissions and External Costs: 2004–Early 2005 Status. *Prog. Photovolt. Res. Appl.* **2006**, *14*, 275–280. [[CrossRef](#)]
25. Feldman, D.; Barbose, G.; Margolis, R.; Bolinger, M.; Chung, D.; Fu, R.; Seel, J.; Davidson, C.; Darghouth, N.; Wisser, R. *Photovoltaic System Pricing Trends: Historical, Recent, and Near-Term Projections 2015 Edition*; National Renewable Energy Lab. (NREL): Golden, CO, USA, 2015.
26. Feldman, D.; Barbose, G.; Margolis, R.; Wisser, R.; Darghouth, N.; Goodrich, A. *Photovoltaic (PV) Pricing Trends: Historical, Recent, and Near-Term Projections, Sunshot 2012*; Lawrence Berkeley National Lab. (LBNL): Berkeley, CA, USA, 2012.
27. PVinsights PVinsights. Available online: <http://pvinsights.com/> (accessed on 23 August 2023).
28. Tamarack Solar Products Tamarack Solar Top of Pole Mounts. Available online: <https://www.altestore.com/store/solar-panel-mounts/top-of-pole-mounts-for-solar-panels/tamarack-solar-top-of-pole-mounts-6072-cell-solar-panels-p40745/> (accessed on 29 June 2023).
29. TPM3 Pole Mount for Three 60/72 Cell Solar Modules. Available online: <https://www.modernoutpost.com/product/tpm3-pole-mount-for-three-60-72-cell-solar-modules/> (accessed on 23 August 2023).
30. Precedence Research Agrivoltaics Market Is Expected to Increase at a 12.15% of CAGR by 2030. Available online: <https://www.precedenceresearch.com/press-release/agrivoltaics-market> (accessed on 23 August 2023).
31. International Energy Agency Solar. Available online: <https://www.iea.org/energy-system/renewables/solar-pv> (accessed on 23 August 2023).
32. Dupraz, C.; Marrou, H.; Talbot, G.; Dufour, L.; Nogier, A.; Ferard, Y. Combining Solar Photovoltaic Panels and Food Crops for Optimising Land Use: Towards New Agrivoltaic Schemes. *Renew. Energy* **2011**, *36*, 2725–2732. [[CrossRef](#)]
33. Guerin, T.F. Impacts and Opportunities from Large-Scale Solar Photovoltaic (PV) Electricity Generation on Agricultural Production. *Environ. Qual. Manag.* **2019**, *28*, 7–14. [[CrossRef](#)]
34. Valle, B.; Simonneau, T.; Sourd, F.; Pechier, P.; Hamard, P.; Frisson, T.; Ryckewaert, M.; Christophe, A. Increasing the Total Productivity of a Land by Combining Mobile Photovoltaic Panels and Food Crops. *Appl. Energy* **2017**, *206*, 1495–1507. [[CrossRef](#)]
35. Mavani, D.D.; Chauhan, P.M.; Joshi, V. Beauty of Agrivoltaic System Regarding Double Utilization of Same Piece of Land for Generation of Electricity & Food Production. *Int. J. Sci. Eng. Res.* **2019**, *10*, 118–148.
36. Sekiyama, T.; Nagashima, A. Solar Sharing for Both Food and Clean Energy Production: Performance of Agrivoltaic Systems for Corn, A Typical Shade-Intolerant Crop. *Environments* **2019**, *6*, 65. [[CrossRef](#)]

37. Agostini, A.; Colauzzi, M.; Amaducci, S. Innovative Agrivoltaic Systems to Produce Sustainable Energy: An Economic and Environmental Assessment. *Appl. Energy* **2021**, *281*, 116102. [CrossRef]
38. Daniels, T.L. The Development of Utility-Scale Solar Projects on US Agricultural Land: Opportunities and Obstacles. *Socio-Ecol. Pract. Res.* **2023**, *5*, 205–213. [CrossRef]
39. Wittbrodt, B.; Laureto, J.; Tymrak, B.; Pearce, J.M. Distributed Manufacturing with 3-D Printing: A Case Study of Recreational Vehicle Solar Photovoltaic Mounting Systems. *J. Frugal Innov.* **2015**, *1*, 1. [CrossRef]
40. Wittbrodt, B.T.; Pearce, J.M. Total U.S. Cost Evaluation of Low-Weight Tension-Based Photovoltaic Flat-Roof Mounted Racking. *Sol. Energy* **2015**, *117*, 89–98. [CrossRef]
41. Wittbrodt, B.; Pearce, J.M. 3-D Printing Solar Photovoltaic Racking in Developing World. *Energy Sustain. Dev.* **2017**, *36*, 1–5. [CrossRef]
42. Arefeen, S.; Dallas, T. Low-Cost Racking for Solar Photovoltaic Systems with Renewable Tensegrity Structures. *Sol. Energy* **2021**, *224*, 798–807. [CrossRef]
43. Pearce, J.M.; Meldrum, J.; Osborne, N. Design of Post-Consumer Modification of Standard Solar Modules to Form Large-Area Building-Integrated Photovoltaic Roof Slates. *Designs* **2017**, *1*, 9. [CrossRef]
44. Vandewetering, N.; Hayibo, K.S.; Pearce, J.M. Impacts of Location on Designs and Economics of DIY Low-Cost Fixed-Tilt Open Source Wood Solar Photovoltaic Racking. *Designs* **2022**, *6*, 41. [CrossRef]
45. Vandewetering, N.; Hayibo, K.S.; Pearce, J.M. Open-Source Design and Economics of Manual Variable-Tilt Angle DIY Wood-Based Solar Photovoltaic Racking System. *Designs* **2022**, *6*, 54. [CrossRef]
46. Vandewetering, N.; Hayibo, K.S.; Pearce, J.M. Open-Source Vertical Swinging Wood-Based Solar Photovoltaic Racking Systems. *Designs* **2023**, *7*, 34. [CrossRef]
47. Masna, S.; Morse, S.M.; Hayibo, K.S.; Pearce, J.M. The Potential for Fencing to Be Used as Low-Cost Solar Photovoltaic Racking. *Sol. Energy* **2023**, *253*, 30–46. [CrossRef]
48. Mayville, P.; Patil, N.V.; Pearce, J.M. Distributed Manufacturing of after Market Flexible Floating Photovoltaic Modules. *Sustain. Energy Technol. Assess.* **2020**, *42*, 100830. [CrossRef]
49. Jamil, U.; Vandewetering, N.; Pearce, J.M. Solar Photovoltaic Wood Racking Mechanical Design for Trellis-Based Agrivoltaics. *PLoS ONE* **2023**, *18*, e0294682. [CrossRef] [PubMed]
50. Franz, J.; Morse, S.; Pearce, J.M. Low-Cost Pole and Wire Photovoltaic Racking. *Energy Sustain. Dev.* **2022**, *68*, 501–511. [CrossRef]
51. Lehmann, S. Sustainable Construction for Urban Infill Development Using Engineered Massive Wood Panel Systems. *Sustainability* **2012**, *4*, 2707–2742. [CrossRef]
52. We Explain Why Wood Is Eco Friendly and a Sustainable Material. Available online: <https://www.woodchoose.com/> (accessed on 18 October 2023).
53. ItTakesAForest #ItTakesAForest. Available online: <https://ittakesaforest.ca/people-products/wood-making-our-lives-better/> (accessed on 18 October 2023).
54. Circular Ecology. *Embodied Carbon Footprint Database*; Circular Ecology: Worcester, UK, 2023; Available online: <https://circularecology.com/embodied-carbon-footprint-database.html> (accessed on 18 October 2023).
55. Rana, S.; Vandewetering, N.; Powell, J.; Ariza, J.Á.; Pearce, J.M. Geographical Dependence of Open Hardware Optimization: Case Study of Solar Photovoltaic Racking. *Technologies* **2023**, *11*, 62. [CrossRef]
56. Galvanized Aircraft Cable 7x19, 1/4 in. x 200 Feet. Available online: <https://www.bestmaterials.com/detail.aspx?ID=25064> (accessed on 18 October 2023).
57. Heliene 144HC M6 Bifacial Module 144 Half-Cut Monocrystalline 440W–460W (HSPE-144HC-M6-Bifacial-Rev.05.Pdf) 2022. Available online: <https://heliene.com/144hc-m6-monofacial-module/> (accessed on 18 October 2023).
58. Molin, E.; Stridh, B.; Molin, A.; Wäckelgård, E. Experimental Yield Study of Bifacial PV Modules in Nordic Conditions. *IEEE J. Photovolt.* **2018**, *8*, 1457–1463. [CrossRef]
59. Riedel-Lyngskær, N.; Ribaconka, M.; Pó, M.; Thorseth, A.; Thorsteinsson, S.; Dam-Hansen, C.; Jakobsen, M.L. The Effect of Spectral Albedo in Bifacial Photovoltaic Performance. *Sol. Energy* **2022**, *231*, 921–935. [CrossRef]
60. Hayibo, K.S. Monofacial vs Bifacial Solar Photovoltaic Systems in Snowy Environments. *Renew. Energy* **2022**, *193*, 657–668. [CrossRef]
61. Russell, A.C.J.; Valdivia, C.E.; Haysom, J.E.; Hinzer, K. Impact of Snow Depth on Single-Axis Tracked Bifacial Photovoltaic System Performance. In Proceedings of the 2022 IEEE 49th Photovoltaics Specialists Conference (PVSC), Philadelphia, PA, USA, 5–10 June 2022; pp. 1–4.
62. Heidari, N.; Gwamuri, J.; Townsend, T.; Pearce, J.M. Impact of Snow and Ground Interference on Photovoltaic Electric System Performance. *IEEE J. Photovolt.* **2015**, *5*, 1680–1685. [CrossRef]
63. Rigging Canada 3/8" x 500 Galvanized Aircraft Cable. Available online: <https://riggingcanada.ca/store/wire-rope-and-aircraft-cable/aircraft-cable/aircraft-cable-7x19-galvanized/38-x-500-galvanized-aircraft-cable/> (accessed on 18 October 2023).
64. Sadat, S.A.; Vandewetering, N.; Pearce, J.M. Mechanical and Economic Analysis of Conventional Aluminum Photovoltaic Module Frames, Frames with Side Holes, and Open-Source Downward-Fastened Frames for Non-Traditional Racking. *J. Sol. Energy Eng.* **2023**, *146*, 025001. [CrossRef]
65. Beinert, A.J.; Romer, P.; Heinrich, M.; Mittag, M.; Aktaa, J.; Neuhaus, D.H. The Effect of Cell and Module Dimensions on Thermomechanical Stress in PV Modules. *IEEE J. Photovolt.* **2020**, *10*, 70–77. [CrossRef]

66. Tummalieh, A.; Beinert, A.J.; Reichel, C.; Mittag, M.; Neuhaus, H. Holistic Design Improvement of the PV Module Frame: Mechanical, Optoelectrical, Cost, and Life Cycle Analysis. *Prog. Photovolt. Res. Appl.* **2022**, *30*, 1012–1022. [CrossRef]
67. CanmetENERGY/Housing, Buildings and Communities National Resources Canada Solar Ready Guidelines. 2013. Available online: <https://natural-resources.canada.ca/energy-efficiency/data-research-insights-energy-ef/housing-innovation/solar-ready-guidelines/5141> (accessed on 18 June 2023).
68. 2018 NDS. Available online: <https://awc.org/publications/2018-nds/> (accessed on 18 June 2023).
69. Greentech Renewables Solar PV Racking Options—Comparison Chart | Greentech Renewables. Available online: <https://www.greentechrenewables.com/article/solar-pv-racking-options-comparison-chart> (accessed on 1 November 2023).
70. Vandewetering, N.; Hayibo, K.S.; Pearce, J.M. Open-Source Photovoltaic—Electrical Vehicle Carport Designs. *Technologies* **2022**, *10*, 114. [CrossRef]
71. MarketWatch 2023 Guide to Solar Carports: Are They Worth It? Available online: <https://www.marketwatch.com/guides/solar/solar-carport/> (accessed on 6 November 2023).
72. SunWatts Solar Carport Mount. Available online: <https://sunwatts.com/carport-mounts/> (accessed on 6 November 2023).
73. Feldman, D.; Ramasamy, V.; Fu, R.; Ramdas, A.; Desai, J.; Margolis, R. *U.S. Solar Photovoltaic System and Energy Storage Cost Benchmark (Q1 2020)*; National Renewable Energy Lab. (NREL): Golden, CO, USA, 2021.
74. Wüstenhagen, R.; Wolsink, M.; Bürer, M.J. Social Acceptance of Renewable Energy Innovation: An Introduction to the Concept. *Energy Policy* **2007**, *35*, 2683–2691. [CrossRef]
75. Batel, S.; Devine-Wright, P.; Tangeland, T. Social Acceptance of Low Carbon Energy and Associated Infrastructures: A Critical Discussion. *Energy Policy* **2013**, *58*, 1–5. [CrossRef]
76. Calvert, K.; Mabee, W. More Solar Farms or More Bioenergy Crops? Mapping and Assessing Potential Land-Use Conflicts among Renewable Energy Technologies in Eastern Ontario, Canada. *Appl. Geogr.* **2015**, *56*, 209–221. [CrossRef]
77. Sovacool, B.K. Exploring and Contextualizing Public Opposition to Renewable Electricity in the United States. *Sustainability* **2009**, *1*, 702–721. [CrossRef]
78. Sovacool, B.K.; Lakshmi Ratan, P. Conceptualizing the Acceptance of Wind and Solar Electricity. *Renew. Sustain. Energy Rev.* **2012**, *16*, 5268–5279. [CrossRef]
79. Dias, L.; Gouveia, J.P.; Lourenço, P.; Seixas, J. Interplay between the Potential of Photovoltaic Systems and Agricultural Land Use. *Land Use Policy* **2019**, *81*, 725–735. [CrossRef]
80. Pearce, J.M. Agrivoltaics in Ontario Canada: Promise and Policy. *Sustainability* **2022**, *14*, 3037. [CrossRef]
81. Jamil, U.; Hickey, T.; Pearce, J.M. Solar Energy Modelling and Proposed Crops for Different Types of Agrivoltaics Systems. Available SSRN 4579628 **2023**. [CrossRef]
82. Singh, K.; Mishra, S.; Kumar, M.N. A Review on Power Management and Power Quality for Islanded PV Microgrid in Smart Village. *Indian J. Sci. Technol.* **2017**, *10*, 1–4. [CrossRef]
83. Saleh, M.S.; Althabani, A.; Esa, Y.; Mhandi, Y.; Mohamed, A.A. Impact of Clustering Microgrids on Their Stability and Re-Silience during Blackouts. In Proceedings of the 2015 International Conference on Smart Grid and Clean Energy Technologies, ICSGCE, Offenburg, Germany, 20–23 October 2015; pp. 195–200.
84. Record Volatility Presides Over the Lumber Market. Available online: <http://www.contractlumber.com/blog/2021/9/3/record-volatility-presides-over-the-lumber-market> (accessed on 13 November 2023).
85. JuliaSeth Pressure Treated Lumber Prices 2015 vs. 2021. *r/halifax*. 2021. Available online: https://www.reddit.com/r/halifax/comments/mp2cl0/pressure_treated_lumber_prices_2015_vs_2021/ (accessed on 18 October 2023).
86. What Is Driving Price Volatility in the Wood Products Industry? *Fastmarkets*. 2022. Available online: <https://www.fastmarkets.com/insights/price-volatility-drivers-in-wood-products-industry/> (accessed on 18 October 2023).
87. Municipal Climate Change Action Center Solar Friendly Municipalities—Permit Taxes 2019. Available online: <https://mccac.ca/wp-content/uploads/SolarFriendlyMunicipalities-PermitTaxes.pdf> (accessed on 18 October 2023).
88. Toronto, C. of Solar Permitting & Regulations. Available online: <https://www.toronto.ca/services-payments/water-environment/net-zero-homes-buildings/solar-to/solar/> (accessed on 27 November 2023).
89. Solar Panels. Available online: <https://www.waterloo.ca/en/living/solar-panels.aspx> (accessed on 27 November 2023).
90. Building Permits | City of London. Available online: <https://london.ca/living-london/building-renovating/building-permits> (accessed on 29 November 2023).
91. Weisser, D. A Guide to Life-Cycle Greenhouse Gas (GHG) Emissions from Electric Supply Technologies. *Energy* **2007**, *32*, 1543–1559. [CrossRef]
92. Muteri, V.; Cellura, M.; Curto, D.; Franzitta, V.; Longo, S.; Mistretta, M.; Parisi, M.L. Review on Life Cycle Assessment of Solar Photovoltaic Panels. *Energies* **2020**, *13*, 252. [CrossRef]
93. Kim, J.; Rabelo, M.; Padi, S.P.; Yousuf, H.; Cho, E.-C.; Yi, J. A Review of the Degradation of Photovoltaic Modules for Life Expectancy. *Energies* **2021**, *14*, 4278. [CrossRef]
94. Aghaei, M.; Fairbrother, A.; Gok, A.; Ahmad, S.; Kazim, S.; Lobato, K.; Oreski, G.; Reinders, A.; Schmitz, J.; Theelen, M.; et al. Review of Degradation and Failure Phenomena in Photovoltaic Modules. *Renew. Sustain. Energy Rev.* **2022**, *159*, 112160. [CrossRef]
95. Joist Hangers and End Moments—Structural Engineering General Discussion—Eng-Tips. Available online: <https://www.eng-tips.com/viewthread.cfm?qid=339938> (accessed on 27 August 2023).

-
96. National Research Council Canada, National Building Code of Canada 2020. 2022. Available online: <https://nrc.canada.ca/en/certifications-evaluations-standards/codes-canada/codes-canada-publications/national-building-code-canada-2020> (accessed on 18 October 2023).
 97. Dead Loads. Available online: https://www.designingbuildings.co.uk/wiki/Dead_loads (accessed on 18 June 2023).

Disclaimer/Publisher's Note: The statements, opinions and data contained in all publications are solely those of the individual author(s) and contributor(s) and not of MDPI and/or the editor(s). MDPI and/or the editor(s) disclaim responsibility for any injury to people or property resulting from any ideas, methods, instructions or products referred to in the content.